Axis-Symmetric Ram Accelerator Projectile Performance Characteristics

Sizhe Liu

A thesis submitted in partial fulfillment of the

requirements for the degree of

Master of Science in Aeronautics & Astronautics

University of Washington

2019

Committee:

Carl Knowlen

Robert Breidenthal

Program Authorized to Offer Degree:

Aeronautics and Astronautics

University of Washington

Abstract

Axis-Symmetric Ram Accelerator Projectile Performance Characteristics

Sizhe Liu

Chair of the Supervisory Committee:
Professor Carl Knowlen
Aeronautics and Astronautics

The railed-tube ram accelerator is a launch device capable of accelerating a projectile to hypersonic speed. The device has the potential for future space launch and the current application involves oil drilling and tunnel drilling. The railed-tube ram accelerator is a derivative of a smooth-bore ram accelerator in that it uses a railed-tube insert to guide and stabilize the projectiles without the need to utilize finned projectiles. The initial experiments on the prototype railed-tube ram accelerator with axis-symmetric projectiles at entrance velocity of 1030 m/s have demonstrated acceleration up to a velocity of 1120 m/s using a propellant mixture of 1.0 CH_4 + 9.52 Air at 16-atm fill pressure. The velocity gain of 90 m/s across the 2-m-long railed-tube ram accelerator corresponds to an average acceleration of 4,900 g. Compared to the theoretical performance model of the thermally-choked ram accelerator, the prototype railed-tube ram accelerator only produces a fraction of the predicted thrust. Gasdynamic starting of the projectile was observed at velocities as low as ~800 m/s, which indicates the potential for ram accelerator starting at low velocities in railed-tubes.

Contents

LIST OF FIGURES i

LIST OF TABLES iii

NOMENCLATURE iv

LIST OF ABBREVIATIONS vi

ACKNOWLEDGEMENTS vii

DEDICATION ix

CHAPTER 1: INTRODUCTION 1

Smooth-Bore Ram Accelerator 1

Baffled-Tube Ram Accelerator 4

Railed-Tube Ram Accelerator 5

Starting Envelope of the TCRA 6

CHAPTER 2: THEORETICAL MODELS 11

Thermally-Choked Ram Accelerator 11

Smooth Bore TCRA Limitations 17

Baffled-Tube Ram Accelerator 19

Baffled-Tube Ram Accelerator Performance Model 20

Normal Shock System Location Prediction Methodology 23

CHAPTER 3: EXPERIMENTAL APPARATUS AND METHODOLOGY 28

Experiment Facility 28

Experimental Set-up 28

Gas Handling 32

Railed-Tube Design 33

Centering Ring Design 37

Projectile & Piston Configuration 41

RTRA Experimental Procedure 45

CHAPTER 4: EXPERIMANTAL RESULTS AND DISCUSSION 48

Collection and Processing of Raw Experimental Data 48

Railed-Tube Ram Accelerator Data Analysis 49

CHAPTER 5: CONCLUSION 65

Future Work 65

BIBLIOGRAPHY 67

LIST OF FIGURES

Figure 1. 1: Conventional ramjet schematic 2
Figure 1. 2: Thermally-choked ram accelerator propulsive cycle 3
Figure 1. 3: Normal baffled-tube ram accelerator schematic 4
Figure 1. 4: Railed-tube ram accelerator schematic..... 5
Figure 1. 5: Successful start 7
Figure 1. 6: Sonic diffuser unstart..... 7
Figure 1. 7: Wave fall-off 7
Figure 1. 8: Wave unstart..... 7
Figure 1. 9: Generalized starting envelope of the TCRA 9
Figure 1. 10: Start attempt results with varying throat flow area in nitrogen-diluted propellants 10

Figure 2. 1: Smooth-Bore Ram Accelerator Control Volume 12
Figure 2. 2: Smooth Bore TCRA non-dimensional thrust envelope..... 15
Figure 2. 3: Smooth-bore TCRA experiment-theory correlation velocity profile at optimized gas mixtures..... 17
Figure 2. 4: Theoretical operation window for smooth bore TCRA..... 19
Figure 2. 5: Normal baffled-tube schematic 20
Figure 2. 6: Schematic of baffle effective area 21
Figure 2. 7: Baffled-tube TCRA model at various drag coefficients (Q = 12)..... 22
Figure 2. 8: Thermally-choked ram accelerator propulsive mode with station numbers 24

Figure 3. 1: Light gas gun schematic 29
Figure 3. 2: Schematic of the ram accelerator in University of Washington..... 31
Figure 3. 3: Rails of the prototype RTRA..... 36
Figure 3. 4: Rail design part drawing..... 37
Figure 3. 5: Baffle local buckling 38
Figure 3. 6: Centering ring part drawing 39
Figure 3. 7: Shell tube with 3” bore and its railed-tube insert 40

Figure 3. 8: Railed-Tube insert Assembly Part Drawing 41
Figure 3. 9: Axis-symmetric projectile part drawing 43
Figure 3. 10: Obturator (Piston) part drawing 44
Figure 3. 11: Lexan projectile and piston for the prototype RTRA 45

Figure 4. 1: RTRA shock reflection schematic 52
Figure 4. 2: HS2080 pressure plot at station 6 52
Figure 4. 3: HS2080 pressure plot at station 7 52
Figure 4. 4: Pressure plot of HS2081 at station 8 53
Figure 4. 5: Pressure plot of HS2080 at station 9 53
Figure 4. 6: HS2079 pressure plot at station 6 55
Figure 4. 7: BTRA pressure plot with combustion activity (pressure signal at station 6 in HS2078) 56
Figure 4. 8: Pressure profile of firing no. 263 in ISL 57
Figure 4. 9: HS2083 pressure plot at station 6 58
Figure 4. 10: HS2083 pressure plot at station 7 58
Figure 4. 11: HS2085 pressure plot at station 7 59
Figure 4. 12: HS2085 pressure plot at station 8 59
Figure 4. 13: RTRA railed-tube insert and shell tube failure surface 61
Figure 4. 14: TCRA theoretical thrust/heat release-Mach curve (1.0 CH4 + 9.52 Air; P = 150psi/10atm) 64
Figure 4. 15: Non-dimensional heat release of the RTRA propellants 64

LIST OF TABLES

Table 3. 1: Test section configuration..... 30
Table 3. 2: Instrumentation ports location and sensors (red stations in RTRA)..... 31

Table 4. 1: Initial RTRA experiment result 50
Table 4. 2: Propellants properties 50

NOMENCLATURE

Variables

β - Volume Void Ratio

Q – Non-Dimensional Heat Release

AR - Aspect Ratio

γ - Specific Heat Ratio

ρ - Density

A - Area

a - Acceleration

a - Acoustic Speed

C_p Specific Heat Capacity at Constant Pressure

C_v Specific Heat Capacity at Constant Volume

T - Temperature

R – Radius

D - Diameter

F - Thrust Force

h - enthalpy

I - Non-Dimensional Thrust

L - Length

M - Mach Number

m - Mass

P – Pressure

LIST OF ABBREVIATIONS

CAD: Computer Aided Design

CFD: Computational Fluid Dynamics

CJ: Chapman-Jouguet

EM: Electromagnetic

FEA: Finite Element Analysis

MFC: Mass Flow Controller

SBRA: Smooth Bore Ram Accelerator

TCRA: Thermally-Choke Ram Accelerator

BTRA: Baffled-Tube Ram Accelerator

RTRA: Railed-Tube Ram Accelerator

UW: University of Washington

ACKNOWLEDGEMENTS

First, I would like to thank my advisor Prof. Carl Knowlen for offering me the opportunity to work on different ram accelerator projects since I became a volunteer in the ram accelerator lab. I still remember the first day I came into the ram accelerator lab before the Fall Quarter 2017 started. Everything in the lab looked like an alien artifact to me! (And the lab hygiene condition was a mess back then, though now it got much better.) I still remember the first time Prof Knowlen showed me what a ram accelerator was and I got to see all the souvenir broken diaphragms, armor steel plate and prototype projectiles that day. I felt like I was the most stupid engineer in the world after the first visit and unable to work on such advanced aerospace project. However, Prof Knowlen always encouraged me that I could do this! No matter how repetitive my questions were, Prof Knowlen was always very patient to answer them, though I had mistaken ram accelerator as a gun for a long time. I have learned invaluable lessons about gasdynamics, design, engineering analysis and ram accelerator from the time I worked with Prof. Knowlen. More importantly, Prof. Knowlen has prepared me to be a better engineer in every way. Also, I would like to thank Prof. Robert Breidenthal for giving me feedback on my work with the railed-tube ram accelerator.

A special thanks to Trever Byrd for showing me how to operate different components of the ram accelerator lab and always there to answer my questions no matter how repetitive they were. With his help, I was able to understand how to conduct a successful ram accelerator experiment and guarantee the safety during each shot. Navid Daneshvaran for his CFD analysis on the baffled-tube ram accelerator. His simulation gave me an insight of the flow dynamics in RTRA, a similar system to BTRA, and I was able to use it as a guidance to design the prototype railed-tube insert for the RTRA. Brian Leege for his help in data collection, analysis and railed-

tube design. With his work, I was able to interpret the raw data from each shot and understood the limitation and gasdynamics of the prototype RTRA. Hypersciences Inc. for their generous financial support. Without their funding, the prototype railed-tube ram accelerator design, manufacturing, and the exploration of RTRA performance would not be possible. Thanks to Hypersciences' support and vision, we were able to become the pioneer in RTRA research in the world.

Last but certainly not least, I would like to thank the research volunteers whom have put countless hours into helping set up for each experiment. Especially Finn van Donkelaar, Christina Dong and Adrian Lo. Their hard work guaranteed the safety and success of every single experiment.

DEDICATION

To the fellow ram accelerator engineers and researchers in the world for always reminding me that I am never alone on the path that I have been pursuing

CHAPTER 1: INTRODUCTION

Ram accelerator is a launch device capable of performing low-orbit space launch by accelerating the projectile/payload to sub-orbital speed with the tailoring of pressures and gases in each section of the system. The ram accelerator propulsive cycles are similar to that of an air-breathing ramjet engine [1]. This device has the potential to reach in excess of 6 km/s, although to date the ram accelerator has only demonstrated muzzle velocities up to 2.6 km/s in the laboratory. Traditional space launch is heavily dependent on rocket boosters with a first stage that typically drops off at a velocity of 2.0 - 2.5 km/s. The first stage of a typical rocket booster requires a large fuel tank, which accounts for majority of the weight of the rocket system. With ram accelerator, the projectile can be accelerated to first stage separation speed at the ground level. Being inherently scalable, the ram accelerator can replace the first stage of rocket booster for missions with acceleration insensitive payloads. This allows the mass of payload to be increased significantly. Future application of ram accelerator includes interplanetary launch from planets that have lower escape-velocity than Earth, boring holes through hard rock for resource exploration and extraction, and the percussion drilling of tunnels.

Smooth-Bore Ram Accelerator

The concept of the ram accelerator was first developed at the University of Washington in the 1980s [2]. It has a 38.1-mm-bore, eight 2-m-long sections which result to a length of 16m in total, and holds the maximum muzzle velocity record of 2.6 km/s [3]. Similar ram accelerator systems used to be found in the U.S. Army Research Laboratory (ARL) [4] and French-German Research Institution (ISL) [4], with bore diameters of 120-mm and 90-mm, respectively; however, these

programs have ceased to exist. The ram accelerator cycle is similar to that of an air-breathing ramjet engine, as discussed below.

Conventional air-breathing ramjet (open Brayton Cycle) has a center body with cowling attachment at the center of inlet. Ideally, the incident supersonic air will slow down to just above Mach 1 at the minimum flow area of the diffuser, i.e., its throat. A normal shock forms downstream of the diffuser throat that renders the flow subsonic, acting as a compressor to compress the incident air. Fuel is then injected into the combustion chamber to enable subsonic combustion (Figure 1.1).

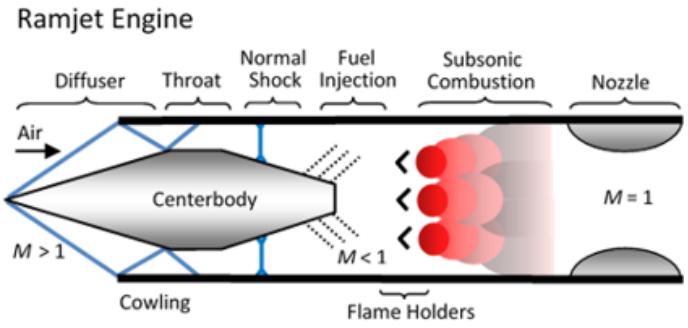

Figure 1. 1: Conventional ramjet schematic

The ram accelerator uses a projectile and a stationary tube wall. Instead of ingesting air from the freestream and fuel injection, the ram accelerator of UW launch a projectile via a gas gun into pre-filled gas mixtures of oxidizer and fuel. Similar to a ramjet, the shock system slows down the flow and subsonic combustion is stabilized behind the projectile (Figure 1.2). The energy released due to the combustion raises the temperature accelerates the flow to a state of thermally choking. This process establishes a normal shock wave (which is often a shock train) on the projectile body. The region between the normal shock system and the thermally-choking state is at very high pressure and this is the driving force of the projectile. When operating the ram accelerator in the thermally

choked ram accelerator (TCRA) propulsive mode, the maximum velocity of the projectile will be limited to, in principle, the Chapman-Jouguet (CJ) detonation speed. The ram accelerator, however, has been shown to reliably operate throughout the trans-detonative velocity regime (±10% CJ speed) and at superdetonative velocities (> 110% CJ speed) [3].

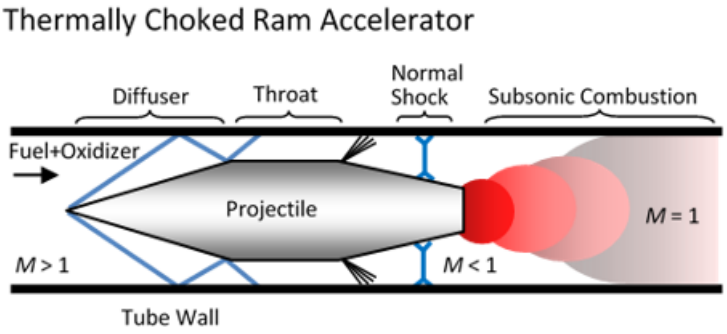

Figure 1. 2: Thermally-choked ram accelerator propulsive cycle

Performance models (thrust vs. Mach number) of SBRA (Smooth Bore Ram Accelerator) with different propellants mixtures have been thoroughly explored at the UW [1-3]. SBRA is relatively sensitive to the non-dimensional heat release in the system, Q, which is defined as $Q = \frac{q}{c_p T}$ (where q is the real heat release per unit mass during the combustion, c_p is the specific heat at constant pressure and T is the static temperature of the propellant. Too much Q will result in shock system being driven ahead of the projectile, resulting in an unstart. The 'unstart' means the shock system is pushed ahead of the projectile with flow choked at its throat, causing the projectile nosecone to be exposed to high pressure, subsonic flow only. Not enough heat release, however, will result in shock system falling behind the projectile, which eventually leads to "wave fall-off" and the loss of thrust.

Baffled-Tube Ram Accelerator

The BTRA (baffled-tube ram accelerator) was introduced because of its ability to operate with much greater heat release than the SBRA, and thus has the potential to generate 3 times the SBRA thrust at the same filled pressure [5, 6]. The BTRA has in-tube baffles, acting as one-way valves that obstruct the flow inside the ram accelerator (Figure 1.3). These suppress the forward surging shock system so that more energetic propellants can be used to increase thrust at a given fill pressure. This is an excellent solution to overcome the *Q* limitation of the conventional thermally-choked SBRA. An initial performance model has been proposed by Knowlen et al. [7] based on the performance model of TCRA, which was subsequently advanced by Glusman [8] and Byrd [9]. The model predicted that the thrust at low Mach number would be higher due to a 'negative drag' from the flow moving upstream in the lab frame of reference. Concurrent BTRA experiments [7,10] demonstrated a 30% - 100% increase in thrust with additional 40% - 70% heat release compared to the SBRA at similar fill pressures.

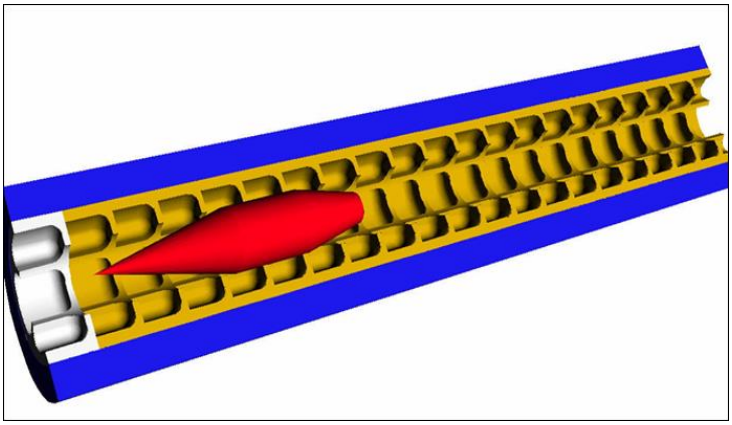

Figure 1. 3: Normal baffled-tube ram accelerator schematic

Railed-Tube Ram Accelerator

Fins are required to stabilize the projectiles in the SBRA. Otherwise, the trajectory of the projectiles will be unpredictable and the projectiles can potentially damage the tube bore. The RTRA, however, uses axis-symmetric projectiles stabilized by internal rails (Figure 1.4). The advantage of axis-symmetric projectiles is that there is more volume aboard for payload and there are no fins exposed to high pressure, reactive flow inside the ram accelerator, which leads to their erosion. In addition, axis-symmetric projectiles are simpler, and thus cheaper, to fabricate, which substantially reduces operating costs of systems designed for rapid firing ram accelerator projectiles. For direct space launch applications, axis-symmetric projectiles are preferred [11,12].

In this project, the operating characteristics of the RTRA with axis-symmetric projectiles were investigated. This is only the 3rd railed-tube ram accelerator for axis-symmetric projectiles built to date that the author is aware of [13,14]. A brief summary of past RTRA programs, the design of the new RTRA, experimental results, and comparisons with theory are presented.

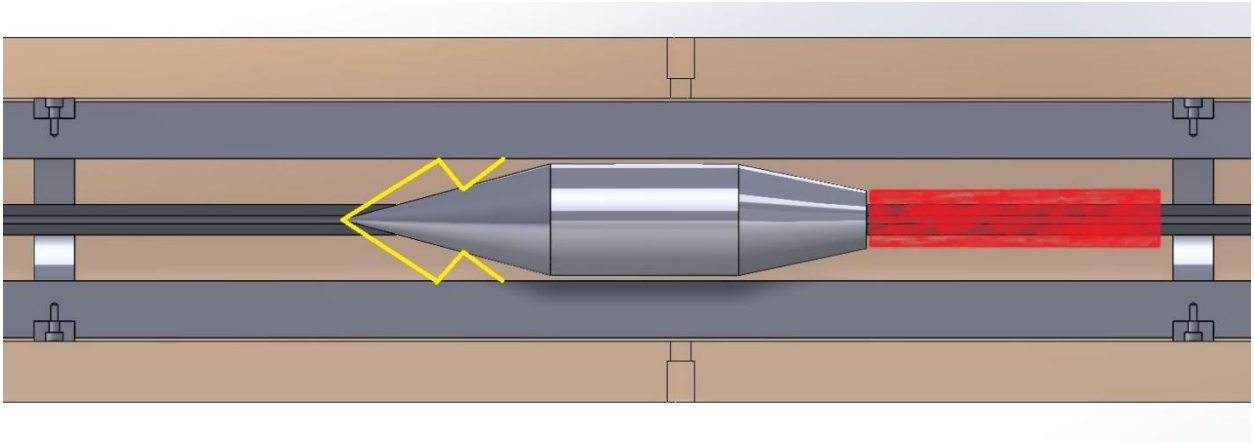

Figure 1. 4: Railed-tube ram accelerator schematic

Starting Envelope of the TCRA

The starting envelope of the TCRA is empirically determined with some gasdynamic and geometric constraints. The starting envelope of the TCRA in UW was first identified and explored by Schultz et al. [15], resulting in the classification of four possible outcomes of a start attempt (Figure 1.5 – 1.8); i.e., successful start, sonic diffuser unstart, wave fall-off, and wave unstart. In order to initiate the ram accelerator process, one first has to accomplish gasdynamic start, which occurs when the flow is at supersonic velocity in the throat region of the projectile (the "throat" is point of maximum projectile cross section and minimum flow passage area). When the entrance Mach number of the ram accelerator is too low, the flow chokes at the projectile throat and a normal shockwave is thereby driven ahead of the projectile (Figure 1.5), resulting in a "sonic diffuser unstart." The effective area ratio ($AR = \frac{A_{projectile}}{A_{flow}}$) or the effective diameter ratio ($DR = \sqrt{AR}$) plays a very important role in establishing the minimum velocity at which a gasdynamic start can be achieved.

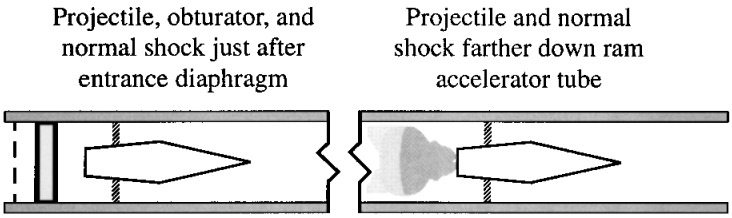

Figure 1. 5: Successful start

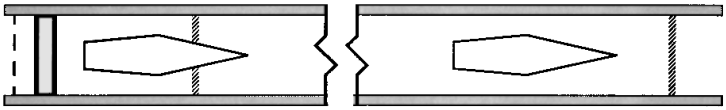

Figure 1. 6: Sonic diffuser unstart

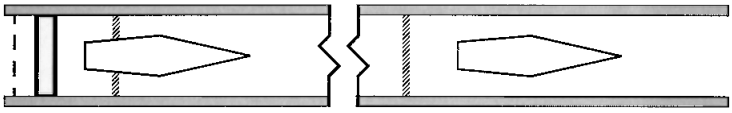

Figure 1. 7: Wave fall-off

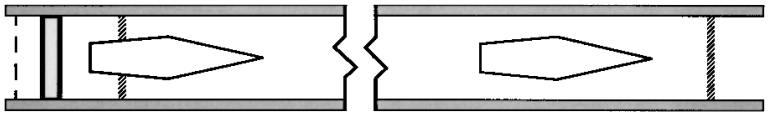

Figure 1. 8: Wave unstart

A wave fall-off unstart relates to not enough heat release from the propellants to keep the normal shock system sitting between the thermally-choked plane and the base of the projectile (Figure 1.7). The projectile will lose acceleration once it outruns the normal shock system in this case because the shock system is the driving force of the projectile. This issue can be resolve by utilizing a more energetic propellant, which effectively increases the *Q* (non-dimensional heat release). A wave unstart will happen, when the normal shock system on aft body of the projectile is disgorged ahead of the diffuser, causing the projectile to decelerate violently. This phenomenon will occur during the starting process when the propellant is too energetic for the ram accelerator system (Figure 1.8).

A successful start is achieved when the system can maintain supersonic flow at the throat of the projectile and the normal shock system is stabilized on the projectile body by thermal choking of the flow at full tube area behind the projectile (Figure 1.5). Note, as the projectile accelerates the total temperature of the flow increases, which can lead to premature combustion of the propellant. If this combustion process moves up onto the projectile body when it is traveling at velocities below CJ speed, the flow can choke on the body and produce an unstart at relatively high Mach number, which is another form of wave unstart. Even though it is a concern, pre-combustion on the nose cone has not yet proven to be a direct cause of unstarts at high Mach numbers [5,6].

Multiple parameters can affect the starting envelop of a TCRA (Figure 1.9). In this project, the key parameter was the throat area, or effective area ratio. Previous study on the TCRA shows that, in a propellant composition range of 2.8 CH_4 + 2.0 O_2 + (4.5-7.5) N_2, a projectile with smaller throat diameter (thus higher flow area) tends to disgorge the shock system at lower *Q*, which then causes unstart. Operation with larger throat flow areas typically requires either reduction of propellant heat release or increase entrance Mach number to contain the shock system. Projectiles with higher throat diameters can contain the shock system better, which allows the use of more energetic propellants provided the entrance Mach number is high enough to accomplish gasdynamic start.

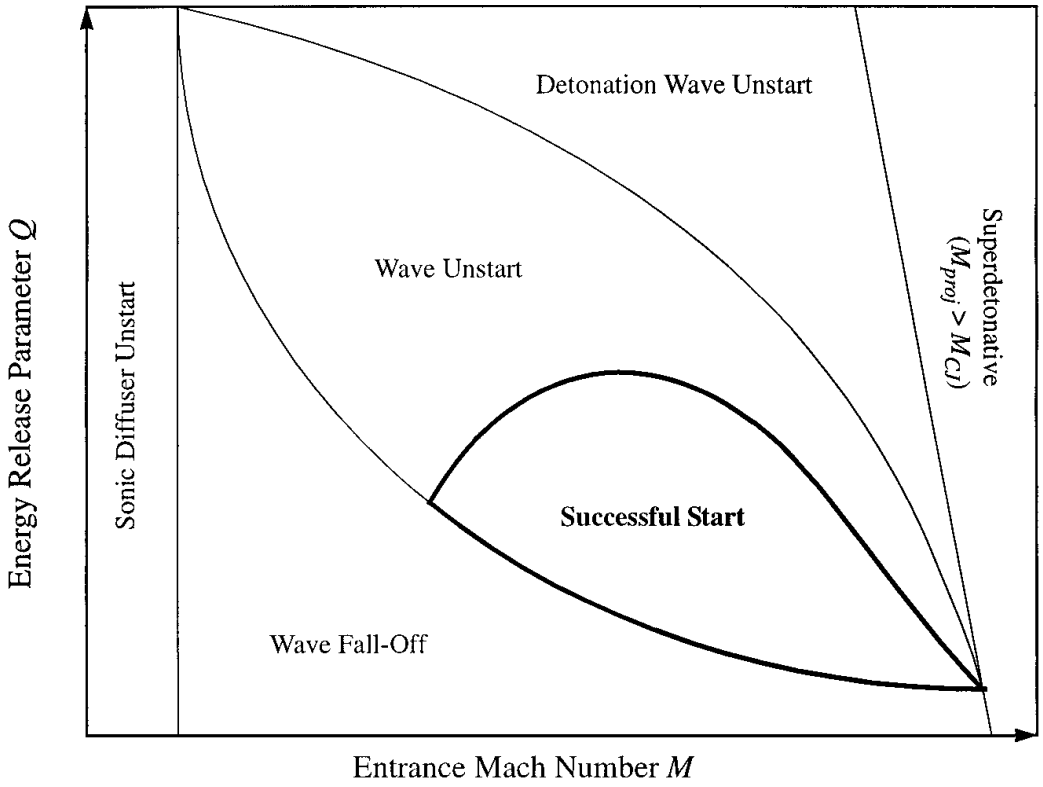

Figure 1. 9: Generalized starting envelope of the TCRA [15].

The starting envelope study done by Schultz et al. [15] considered a nominal throat flow area ratio of 0.42 (A_{throat}/A_{tube}) at a nominal methane/air mixture (fixed Q). In these experiments, the projectile was able to start from Mach 2.9 to 3.6 (Figure 1.10). Projectiles with throat flow ratio less than 0.42 were able to successfully start, showing that a smaller flow area can contain the shock system in this nominal propellant, as long as the diffuser has supersonic flow. However, if the throat flow area is too small, the sonic diffuser unstart Mach number increases, along with the minimum entrance velocity of the projectiles in the ram accelerator system.

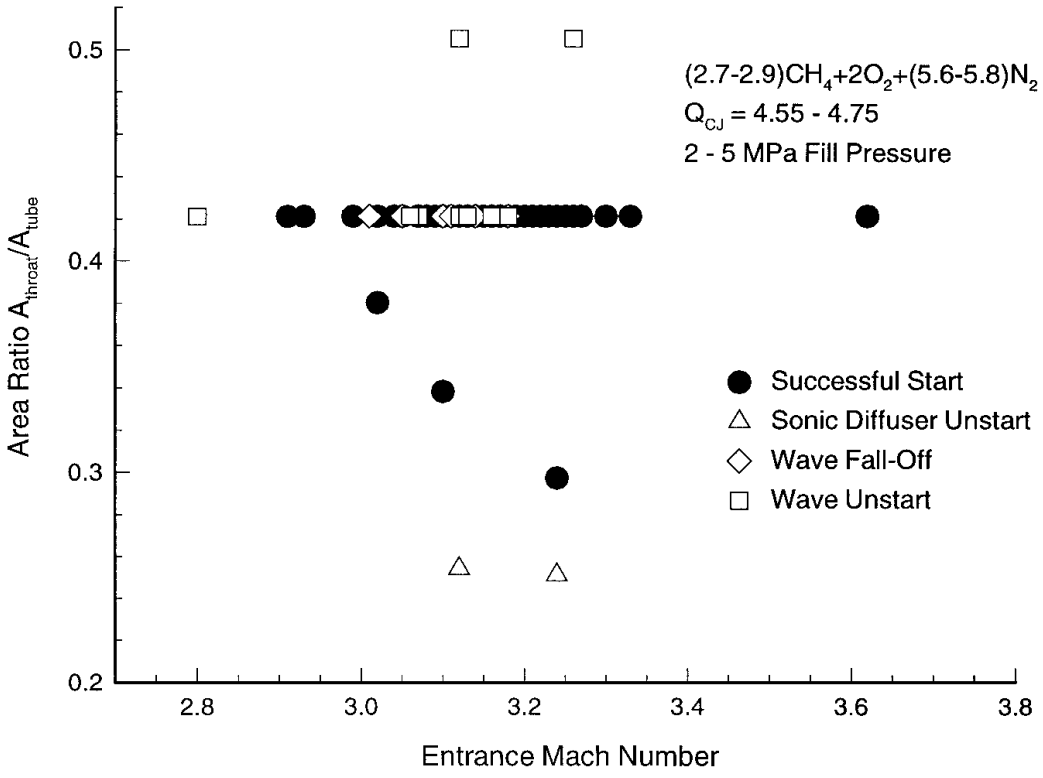

Figure 1. 10: Start attempt results with varying throat flow area in nitrogen-diluted propellants [15].

In the research that is the focus of this thesis, the effective area ratio heavily influenced the design of the rail and centering ring structure. Note that the previous study of starting envelope of the TCRA was conducted in the smooth bore system. While the railed-tube system is not exactly the same, one can apply the starting envelop concept of the smooth bore TCRA to the railed-tube TCRA with the corresponding equivalent area ratios.

CHAPTER 2: THEORETICAL MODELS

This section discusses the theoretical thrust-Mach performance model of the TCRA operating in a smooth bore, and its application to railed-tube and baffled-tube ram accelerators. Acceleration performance in the railed-tube is assumed a priori to be predicted by the original thermodynamic model for the TCRA derived in Refs. [1-3], because the rails inside the RTRA are essentially the cross-section of the fins used on sub-caliber projectiles in the SBRA. The BTRA performance model, however, required inclusion of other flow features not included in the TCRA model, which was investigated in detail by Glusman [8] and subsequently modified by Byrd [9].

Thermally-Choked Ram Accelerator

Thermally-choked ram accelerator operates with a propulsive cycle such that the subsonic combustion/heat addition results a sonic plane sitting behind the projectile; i.e., the combustion process thermally chokes the flow. A normal shock train system is maintained on the aft body of the projectile (often near its base) by the thermal choking, creating a force component to accelerate the projectile. To derive the thrust-Mach performance model of the TCRA, one must make an assumption of one-dimensional flow. The thrust of the TCRA can be determined by the conditions of the upstream (inlet), downstream (at the thermally choked plane) and the subsonic heat addition during the combustion process. Figure 2.1 shows the control volume of the SBRA, where 1 and 2 are the inlet and outlet of the control volume, respectively. The flow characteristics inside the control volume are neglected because the outlet conditions coincides with an entropy extremum, thus the end result is independent of the process by which it is reached. Thus, the thrust of the TCRA can be predicted just knowing the propellant composition and Mach of the projectile, as long as it is operating with the thermally-choked propulsive cycle.

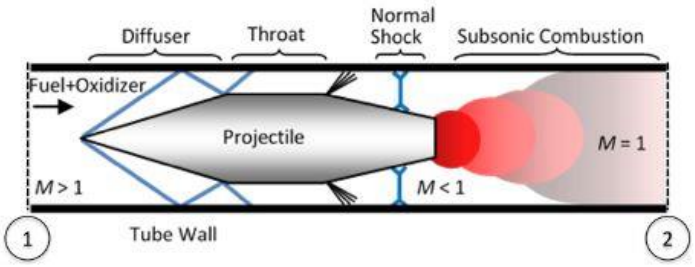

Figure 2. 1: Smooth-Bore Ram Accelerator Control Volume

Applying conservation of momentum to the control volume will result in

$$P_1A_1 + \rho_1{u_1}^2A_1 + F = P_2A_2 + \rho_2{u_2}^2A_2 \quad (2.1)$$

Since the area of the inlet and outlet are the same, the Equation 2.1 is normalized by the cross-section area of the inner tube bore and the pressure at the inlet, P_1.

$$1 + \frac{\rho_1{u_1}^2}{P_1} + \frac{F}{P_1A} = \frac{P_2}{P_1} + \frac{\rho_2{u_2}^2}{P_1} \quad (2.2)$$

Assuming perfect gas such that the local sound speed can be written as $a = \sqrt{\gamma RT}$ and applying ideal gas law ($P = \rho RT$), the Equation 2.2 can be written in terms of Mach number.

$$\frac{F}{P_1A} = \frac{P_2}{P_1}\left(1 + \gamma_2{M_2}^2\right) - \left(1 + \gamma_1{M_1}^2\right) \quad (2.3)$$

Rearrange the Equation 2.3, the equation can now be expressed as the ratio $\frac{P_2}{P_1}$.

$$\frac{P_2}{P_1} = \frac{M_1\sqrt{\gamma_1R_2T_2}}{M_2\sqrt{\gamma_2R_1T_1}} \quad (2.4)$$

Applying the conservation of energy to the control volume, where Δq is the heat addition from inlet to outlet of the control volume, one can get:

$$\rho_1 u_1 A_b \left[h_1 + \frac{{u_1}^2}{2} + \Delta q \right] = \rho_2 u_2 A_b \left[h_2 + \frac{{u_2}^2}{2} \right] \quad (2.5)$$

Then dividing the equation by $\rho_1 u_1$ and applying the conservation of mass results in:

$$h_1 + \frac{{u_1}^2}{2} + \Delta q = h_2 + \frac{{u_2}^2}{2} \quad (2.6)$$

Replacing the velocity terms in terms of Mach number results in:

$$h_1 + \frac{{M_1}^2 \gamma_1 R_1 T_1}{2} + \Delta q = h_2 + \frac{{M_2}^2 \gamma_2 R_2 T_2}{2} \quad (2.7)$$

In order to create non-dimensional variables, the energy equation is normalized by $c_{p1} T_1$ where T_1 is the static temperature of the propellant. This defines a dimensionless heat release term of $Q = \frac{\Delta q}{c_{p1} T_1}$, which turns out to be an independent variable to determine the thrust of SBRA. Rewriting the gas constants and specific heat terms result in the following equation.

$$\frac{h_1}{c_{p1} T_1} + \frac{\gamma_1 - 1}{2} {M_1}^2 + Q = \frac{h_2}{c_{p1} T_1} + \frac{\gamma_2 - 1}{2} {M_2}^2 \frac{c_{p2} T_2}{c_{p1} T_1} \quad (2.8)$$

Rearranging the equation to determine the temperature ratio $\frac{T_2}{T_1}$, one can solve Equation 2.8 in terms of non-dimensional heat release Q and Mach numbers.

$$\frac{T_2}{T_1} = \frac{c_{p1}}{c_{p2}} \left(\frac{Q + \frac{h_1}{c_{p1} T_1} + \frac{\gamma_1 - 1}{2} {M_1}^2}{\frac{h_2}{c_{p2} T_2} + \frac{\gamma_2 - 1}{2} {M_2}^2} \right) \quad (2.9)$$

One can solve the non-dimensional thrust equation for the SBRA by combining Equation 2.9, Equation 2.4 and Equation 2.3.

$$\frac{F}{P_1 A_b} = \frac{M_1 \gamma_1}{M_2 \gamma_2}\left(1 + \gamma_2 {M_2}^2\right)\sqrt{\frac{\gamma_2 - 1}{\gamma_1 - 1}\left(\frac{Q + \frac{h_1}{c_{p1} T_1} + \frac{\gamma_1 - 1}{2}{M_1}^2}{\frac{h_2}{c_{p2} T_2} + \frac{\gamma_2 - 1}{2}{M_2}^2}\right)} - \left(1 + \gamma_1 {M_1}^2\right) \quad (2.10)$$

With the assumption of thermal choking at the outlet of the control volume, the equation can be simplified further. This is the TCRA propulsive mode non-dimensional thrust equation.

$$I_{SBRA} = \frac{F}{P_1 A_b} \quad (2.11)$$

Now that the thrust of the smooth bore TCRA is solely in terms of the heat release and the local Mach number, where the heat release is a function of the propellant at each stage of the ram accelerator, one can plot the thrust vs. local Mach number and non-dimensional heat release. Shown in figure 2.2 is the thrust-heat release-Mach surface of the TCRA thrust equation (Eqn. 2.11). One can see that for a given non-dimensional heat release there is a maximum thrust Mach number and zero thrust number. At the Mach of maximum thrust, the combustion products at the thermal choking point have zero velocity in the lab frame of reference. The zero thrust Mach coincides with the CJ speed of the propellant, at this condition the normal shockwave is predicted to be at the very tip of a sharp tail cone, and thus there is no pressure on the aft body of the projectile to propel it forward. As the heat release increases, the peak thrust and zero thrust Mach numbers increase correspondingly. This effectively widens the operation window of the entire system.

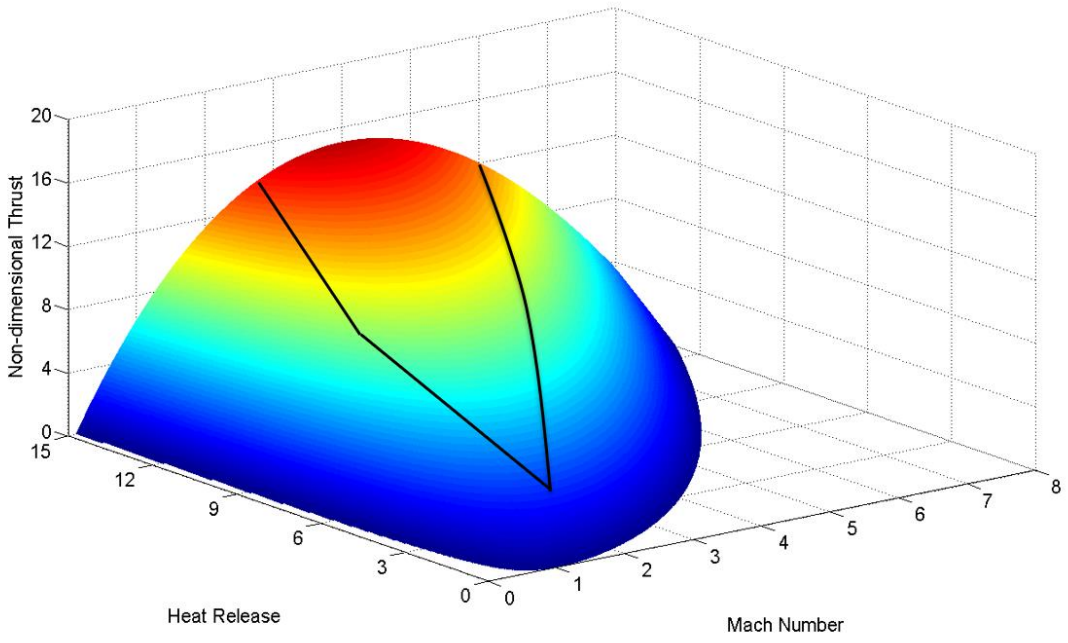

Figure 2. 2: Smooth Bore TCRA non-dimensional thrust envelope

When the SBRA operates in the TCRA propulsive mode, in principle, the projectile in the system could not be accelerated beyond the CJ speed. In order to do so (accelerate beyond CJ speed), one had to operate the SBRA in trans-detonative and/or super-detonative mode [3], which were not considered in this project and are not discussed in detail in this paper. Additionally, the non-dimensional heat release of the smooth bore TCRA is not constant in reality. This is due to the constant change of equilibrium condition, which depends on the in-tube Mach number of the projectile. In this project, the non-dimensional heat release at CJ point (Q_{CJ}) was used as a reference for quantifying the differences in heat release.

As mentioned earlier in this thesis, the smooth bore TCRA thrust-Mach performance model has been thoroughly investigated [1-3]. Multiple gas mixtures have been tested and experimented in the smooth bore TCRA and they all comply with the non-dimensional thrust theory. Figure 2.3

shows one example of such an experiment. In this case, the projectile was accelerated through four stages of the SBRA with each stage containing a different gas mixture. The chosen gas mixtures enabled the projectile to operate at near the maximum thrust Mach number. It can be seen that the correlation between the experiment and theory is excellent. This is considered strong evidence that the thermally-choked assumption for the TCRA non-dimensional thrust performance model is correct.

In the Figure 2.3, there is also shown a theoretical velocity-distance profile where the projectile is operating in a propellant optimized to get the maximum velocity gain over a given distance. All other parameters used for this theoretical result were the same as in the experiment (i.e., fill pressure, weight of projectile and ram accelerator entrance velocity). However, this theoretical acceleration history cannot be accomplished in a SBRA due to the limitations on heat release with which the TCRA can operate. Nevertheless, the differences in velocity-distance profiles show the amount of untapped potential available to the TCRA, should a means to enable it to operate with high-Q-propellants be developed. The thrust-Mach performance model of the smooth-bore TCRA derived above is assumed to be directly applicable to the railed-tube TCRA.

One thing to point out is that the goal of the ram accelerator launch is not to have the projectile accelerate to its maximum operational Mach number in a given gas mixture, though higher Mach number generally means higher speed. Counterintuitively, the projectile should operate at the ‘speed’ (Mach number) where the acceleration is at its maximum. This will allow greater muzzle velocities, but at the expense of using multiple propellant stages. The molecular weight of the gas mixture needs to be decreased as the projectile travels from one stage to another to increase the local sound speed of a gas, and thus keep the in-tube Mach as close to maximum thrust Mach as

possible. However, in this project, this was not an issue because only one 2-meter-long section was filled with energetic propellant.

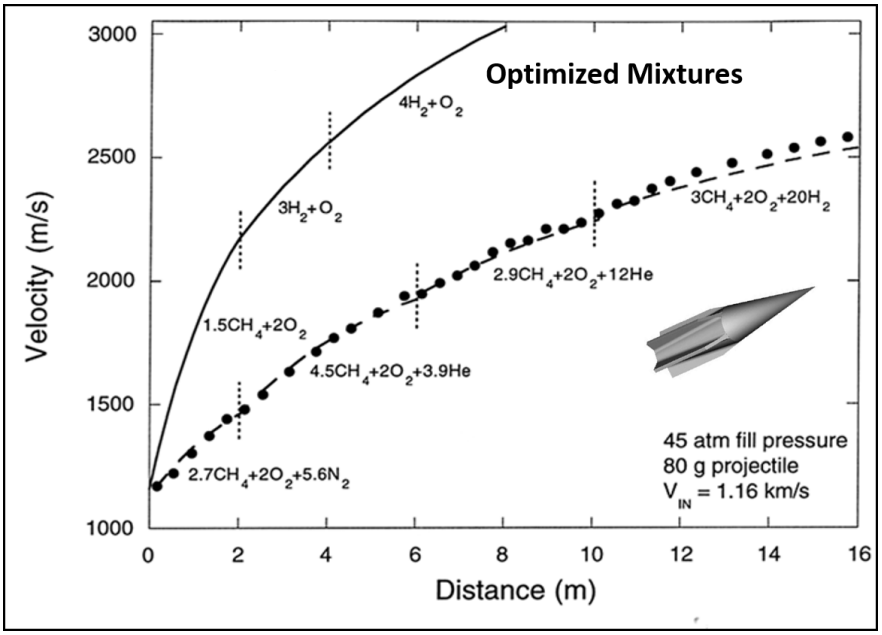

Figure 2. 3: Smooth-bore TCRA experiment-theory correlation velocity profile at optimized gas mixtures [7].

Smooth Bore TCRA Limitations

The derivation of non-dimensional thrust equation for the TCRA does not take into account the flow processes required to accomplish the desired end state of thermal choking, which is one of the most important assumptions made in the control volume analysis and derivation. In a manner similar to the Zel'dovich, von Neumann, Doring (ZND) model for a CJ detonation wave, a one-dimensional flow field model has been proposed to predict the operation limits of the smooth-bore TCRA [16]. This model predicts the minimum ram accelerator entrance velocity corresponds to the supersonic Mach number that results in sonic flow at the projectile throat based on its throat-to-tube flow area ratio with isentropic compression. In Equation 2.12, *A* is the inner tube area and

A^* is the annular area between the bore and the projectile throat, and M is the projectile's in-tube Mach number.

$$\frac{A}{A*} = \frac{1}{M}\left(\frac{\frac{\gamma+1}{2}}{1+\frac{\gamma-1}{2}M^2}\right)^{\frac{\gamma+1}{2(1-\gamma)}} \quad (2.12)$$

The one-dimensional model also predicts the required heat release that is sufficient to stabilize the shock system on the projectile body without driving it passed the throat and that the maximum operational Mach number corresponds to that of the CJ speed. Therefore, there are three limitations on the operation of the smooth bore TCRA, as indicated by the solid lines on the surface plot in Figure 2.2 and as the envelop boundaries in Figure 2.4. These operational boundaries for the smooth-bore TCRA have been explored in $CH_4/O_2/N_2$ and $CH_4/O_2/H_2$ propellants [17,18], and are discussed in more detail below.

The vertical line in Figure 2.4 corresponds to the first limitation, which is the minimum entrance Mach number of the projectile based on a given area ratio. Below this Mach number, the flow will choke at the throat and drive a normal shock ahead of the nose cone, which exposes the entire projectile in a subsonic flow. The second limitation is the maximum heat release of the propellant. Too much heat release will drive the shock system upstream until it surpasses the projectile. As previously mentioned, this phenomenon is called a wave unstart. All unstarts cause high drag on the projectile and cessation of thrust. The third limitation is the minimal heat release required. If there is too little heat release, there will not be enough energy to drive the shock system at the same speed as the projectile as it enters the propellant mixture. This will result in loss of thrust and is called wave fall-off.

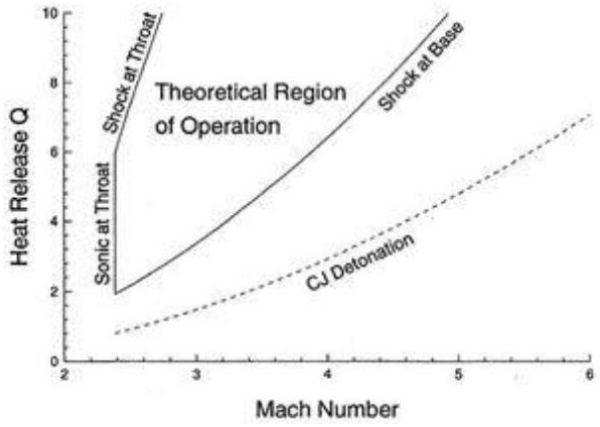

Figure 2. 4: Theoretical operation window for smooth bore TCRA [17].

Based on the Figure 2.4, the minimum Mach number was approximately 2.4 for a projectile with a throat diameter of 29-mm, a tube bore diameter of 38-mm, and a specific heat ratio of 1.4. On the left of the *Region of Operation* is always a projectile unstart while to the right of the *Shock at Base* curve TCRA operation is still observed with bluff based projectiles. One can tailor the gas mixture to meet the operation window by adding either excess fuel or other gases to dilute the mixture since the SBRA is still not capable of running propellant at stoichiometric ratio.

Baffled-Tube Ram Accelerator

In the past research on ram accelerator in UW, lots of work has been put into expanding the operation window of the TCRA. One of the limitations of TCRA is the maximum heat release allowed without unstarting the system. Because the heat release is the driving force of the normal shock wave system, in order to minimize this limitation, one needs to explore a way to mitigate the forward propagation of the shock system. The baffled-tube is such a concept in that each baffle chamber behaves as a one-way valve that allows the in-flow of propellant and prevents forward

surging of the shock system, as shown in Figure 2.5. This solution allows the use of more energetic propellant in the TCRA.

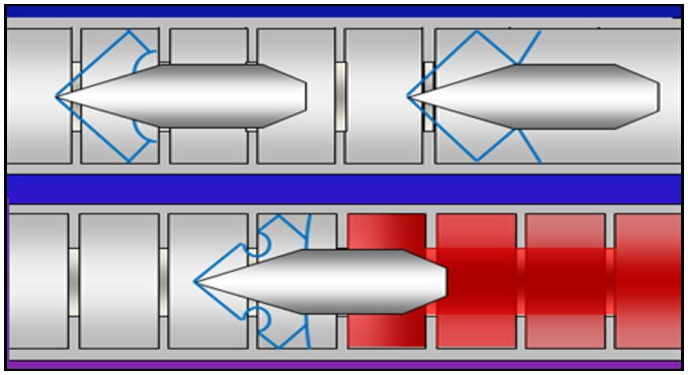

Figure 2. 5: Normal baffled-tube schematic

An additional benefit of baffled-tube concept is that it has the potential to significantly lower the minimum entrance Mach number of the TCRA. Lower entrance velocities reduce the demands on the pre-launcher technology used to provide the projectile's initial acceleration from rest.

Baffled-Tube Ram Accelerator Performance Model

The most recent baffled-tube TCRA performance modeling has been done by Trever Byrd from 2016-2017 [9]. This section provides a summary of the derivation of the baffled-tube TCRA thrust vs. Mach number model and its adaptation to non-circular bore areas. Since baffled-tube ram accelerator has an irregular shaped bore cross-section, an effective area, A_{eff} is introduced. Figure 2.6 shows the schematic of the baffle effective area.

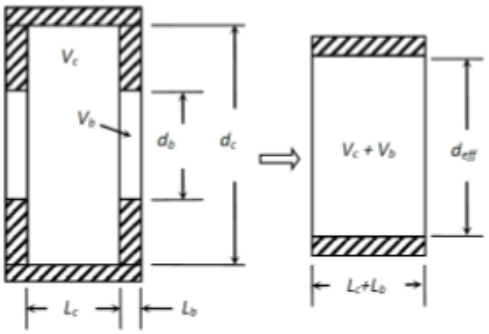

Figure 2. 6: Schematic of baffle effective area

The effective area was defined as:

$$\frac{1}{A_{eff}} = \frac{L_c + L_b}{V_c + V_b} \quad (2.13)$$

where $L_c + L_b$ represents the total length of the baffle and $V_c + V_b$ represents the total volume of the baffles. One can expand the lengths and volumes to get:

$$\frac{1}{A_{eff}} = \frac{L_c + L_b}{V_c + V_b} = \frac{1 + \frac{L_c}{L_b}}{A_b[1 + (\frac{{d_c}^2}{{d_b}^2})(\frac{L_c}{L_b})]} = \frac{1}{A_b\beta} \quad (2.14)$$

By applying the effective area to the non-dimensional thrust equation of the smooth-bore TCRA, one can obtain:

$$I_{BTRA} = \frac{F}{P_1 A_{eff}} = \frac{F}{P_1 A_b \beta} = \frac{I_{SBRA}}{\beta} \quad (2.15)$$

In order to account for the momentum and energy loss of the projectile traveling across the baffles, the non-dimensional equation of the smooth-bore TCRA was re-derived with a drag term as follows:

$$I_{SBRA} = \frac{F}{P_1 A_{eff}}$$

$$= M_1 \frac{\gamma_1}{\gamma_2}(1+\gamma_2)\sqrt{\frac{\gamma_2-1}{\gamma_1-1}\left(\frac{Q+\frac{h_1}{c_{p1}T_1}+\frac{\gamma_1-1}{2}{M_1}^2+\frac{D(\gamma_1-1)}{P_1 A_{eff}\gamma_1}}{\frac{h_2}{c_{p2}T_2}+\frac{\gamma_2-1}{2}}\right)}$$

$$-\left(1+\gamma_1{M_1}^2\right)-\frac{D}{P_1 A_{eff}} \quad (2.16)$$

where the drag term *D* is:

$$D = \frac{1}{2} c_d \rho_1 A_{p,b} n_c |u_1 - u_2|(u_1 - u_2) \quad (2.17)$$

The area term, $A_{p,b}$, accounts the projected area of the baffles vertical to the flow and n_c accounts the number of baffles in the area of interest. Additionally, the velocity term corresponds to the velocity, with respect to the lab, in the high pressure region and the density term is the density of the inlet flow. It is assumed that the drag mainly affects the region between the normal shock system and the thermally-choked plane. Figure 2.7 shows the plots of non-dimensional thrust equation of BTRA with different drag coefficients at Q = 12.

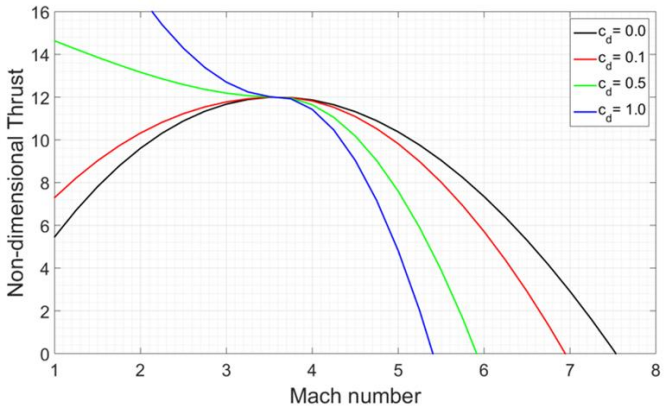

Figure 2. 7: Baffled-tube TCRA model at various drag coefficients (Q = 12)

The BTRA thrust model predicts that there is higher thrust at Mach numbers lower than that of maximum thrust Mach in the TCRA and a lower maximum operational Mach number. At low Mach number, the projectile experiences negative drag because the exhaust products are moving rearward in the lab frame of reference, which results in increased pressure build up on the projectile base. Thus, the projectile experiences more thrust output at low Mach number based on this BTRA performance model.

Normal Shock System Location Prediction Methodology

The projectile in a TCRA is driven by a normal shock system pushed up onto it by the thermally choked combustion process at full tube area behind the projectile. However, in reality, this normal shock system is really a series of compression waves in a shock-train. Because the series of compression waves is nearly equivalent to a single normal shock mathematically, one can simplify the problem by modeling the complicated shock train with a single resultant normal shock. Once the projectile obtains a ram accelerator start, the combustion occurs in the region between the normal shock system and the thermally-choked plane, where the subsonic flow behind the projectile will accelerate to local sonic speed. This combustion process results in a high pressure region to drive the projectile, as long as none of those modes of start failure mentioned in the previous section occurred.

The location of the normal shock system is extremely important. If the normal shock system propagates upstream, surpassing the throat, it will overtake the projectile, causing immediate unstart. If the normal shock system falls back behind the base of the projectile, the projectile will lose thrust because the projectile will no longer be driven by the high-pressure region. To predict the location of the normal shock system, one must first look at a more detailed flow field model, as shown in Figure 2.8.

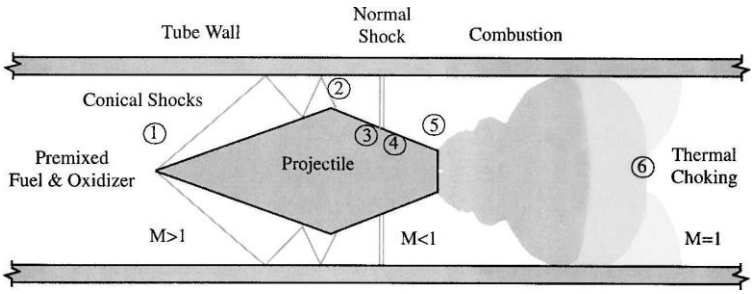

Figure 2. 8: Thermally-choked ram accelerator propulsive mode with station numbers [16].

In the process of estimating the normal shock location, one first makes the following assumptions: Rayleigh flow, perfect gas, and isentropic flow from station 1 to 3 (conical shock pressure losses are negligible at Mach numbers less than 3). In an isentropic process, all total properties are conserved. The normal shock system is a very tiny region where gas properties change dramatically. Across a normal shock wave, the static pressure, temperature and the gas density increase almost instantly. Because normal shock wave does no work to the system and there is no heat addition, the total enthalpy and total temperature remain constant. The static temperature at station 1 is the temperature of the propellant, which is equal to the ambient temperature since there is no pre-heating process being considered here. The total temperature calculations at station 1 are based on the flight Mach number of the projectile (Equation 2.18).

$$T_{t1} = T_1\left(1 + {M_1}^2\frac{\gamma - 1}{2}\right) \quad (2.18)$$

where M_1 is the flight Mach number. Furthermore, the Mach number at the projectile throat (M_2) can be calculated for a known throat-to-tube flow area ratio (Equation 2.19).

$$\frac{A_1}{A_2} = \frac{\left[\frac{1}{M_1}\left(\frac{\frac{\gamma+1}{2}}{1+\frac{\gamma-1}{2}{M_1}^2}\right)^{\frac{\gamma+1}{2(1-\gamma)}}\right]}{\left[\frac{1}{M_2}\left(\frac{\frac{\gamma+1}{2}}{1+\frac{\gamma-1}{2}{M_2}^2}\right)^{\frac{\gamma+1}{2(1-\gamma)}}\right]} \quad (2.19)$$

The total temperatures at station 5 and station 6 are required in order to determine the Mach number at station 5. One can use Rayleigh flow model to estimate the flow conditions at the boundaries of the high-pressure region. There is only one upstream subsonic Mach number in Rayleigh flow control volume with a given heat release. Since the total temperature is constant in regions of isentropic flow and across normal shock wave, the stagnation temperature remains the same from station 1 to station 5.

The combustion process is assumed to be in equilibrium at all Mach numbers. From the TCRA performance derivation previously discussed, the non-dimensional heat release (Q) is applied in constant area region bounded by station 5 at base of projectile and thermal choking plane at station 6 (Equation 2.20):

$$Q = \frac{q_{56}}{C_p T_1} \quad (2.20)$$

where q_{56} is the actual heat release from the propellant based on differences in enthalpy of formation of the combustion products and reactants at 0 K, and C_p is the reactant's specific heat at constant pressure and free stream static temperature. The stagnation temperature at station 6 then can be determined by:

$$T_{06} = T_{05} + QT_1 \quad (2.21)$$

With the stagnation temperature at station 6, one can now determine the Mach number at the upstream of the Rayleigh flow control volume, which is station 5.

$$\frac{T_{06}}{T_{05}} = \left(\frac{1+\gamma {M_5}^2}{1+\gamma {M_6}^2}\right)^2 \left(\frac{{M_6}^2}{{M_5}^2}\right)\left(\frac{1+\frac{\gamma-1}{2}{M_6}^2}{1+\frac{\gamma-1}{2}{M_5}^2}\right) \quad (2.22)$$

To find the normal shock location on the diverging aft body, an iterative process is required. The goal is to find an area ratio where M3 agrees with M4 subject to normal shock jump relations. To start this iterative process, one will first need to guess an area ratio where the normal shock is located. Since the Mach number at throat has been calculated and is only affected by flight Mach number, with the initial guess the area ratio value, one can calculate the Mach number right before the shock (M3) via Equation 2.19. Then, one can use the normal shock relationship to calculate the Mach number right after the shock, M4.

$${M_4}^2 = \frac{(\gamma-1){M_3}^2+2}{2\gamma {M_3}^2-(\gamma-1)} \quad (2.23)$$

The M4 produced from the calculation based on the relation across the normal shock will need to be compared to the M4 produced based on the isentropic flow calculation from station 5 to 4. Because the M5 is determined, one can calculate the M4 via Equation 2.19 (with A_5/A_4). If these values for M4 differ, then the shock is moved to new A_1/A_3 location (note: $A_1/A_3 = A_5/A_4$) and M4 is evaluated again from both shock jump and area expansion relations. This process it repeated until their values for M4 converge. Once the two values of Mach number at station 4 agree, from the resulting area ratio one can readily calculate the location of the normal shock with respect to the throat (or the tip of the nose cone) based on the tapered angle of the projectile. Although this

method does not determine the exact location of the normal shock on the projectile body, it does give an estimation of the location of the region where the normal shock will most likely be in.

CHAPTER 3: EXPERIMENTAL APPARATUS AND METHODOLOGY

This chapter discusses the general layout of the ram accelerator and how the data were collected and processed. In this project, there were three main variables in the experiments: fill pressure, gas mixture and tube configuration. The immediate goals of this experiment were:

- Explore the potential of RTRA system
    - Chemistry/propellants (CH4/Air) – chemistry sweep
    - Ram accelerator filled pressures – pressure sweep
    - Entrance velocity and Mach number – entrance sweep
- Based on experimental performance, determine parameters of a RTRA system that can accelerate a projectile from 1000 m/s to 1600 m/s

Experiment Facility

The experiment facility is located at the Ram Accelerator Laboratory of UW. The launch system is composed of a light gas gun (helium) with a maximum launch speed at around 1200 m/s for 140 g projectile/obturator combinations, eight 2-meter-long tubes with a 38.1 mm bore for a maximum test section length of 16 m, and a gas handling system that can simultaneously deliver three different propellants into the test section. Railed and baffled tube test sections were fabricated in 2-m-lengths so that they can be swapped out with any of the smooth bore tubes in the system.

Experimental Set-up

A helium gas gun (Figure 3.1) was used before the actual ram accelerator section. The gas gun accelerates the projectile to a velocity beyond the minimal entrance velocity such that the projectile

will be able to maintain supersonic flow at its throat. Helium (a_{He} = 1007.4m/s at 293.1K) was used in this light gas gun because of its high local sound speed. Theoretically, a gas gun can accelerate a projectile to up to five times of its gas local sound speed. However, due to barrel friction, in practice, most light gas guns can only accelerate the projectiles to around two times of its gas sound speed as long as there is enough gun pressure and barrel length. The light gas gun in UW Ram Accelerator Laboratory has a maximum muzzle velocity of around 1300 m/s. Hydrogen (a_{H2} = 1306 m/s at 293.15K) is a higher performance choice for gun propellant; however, due to its volatile nature, hydrogen was not used in this project for the purpose of lab safety.

Two sets of 0.32" aluminum diaphragms were used to hold the breech pressure. The breech is a small volume region between two sets of diaphragms and it is filled to certain pressure to regulate the pressure difference across the upstream set of diaphragms. Each diaphragm had an 'X' scribed on one of its surfaces to ensure predictable burst. A hydraulic press was used to score the diaphragm. The score pressure was set to 1000 psi, which affects the pressure at which the diaphragms rupture. Higher score pressure lowers diaphragm rupture pressure.

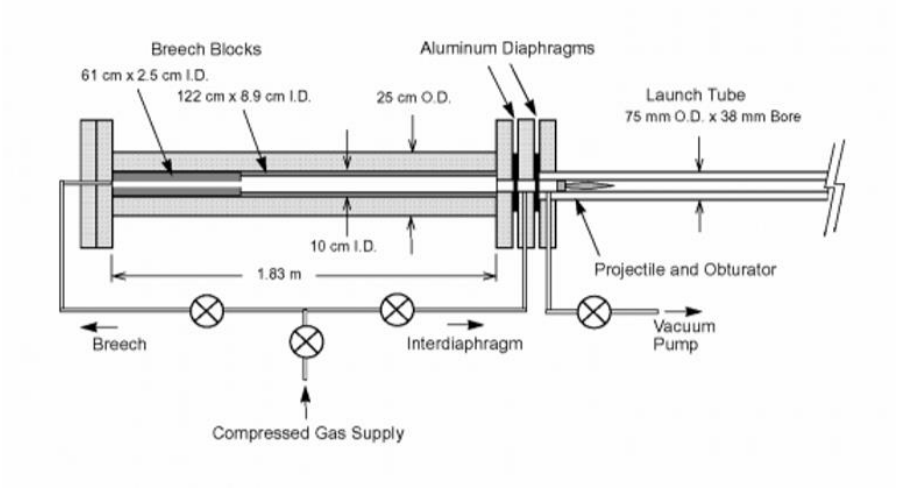

Figure 3. 1: Light gas gun schematic

Each 2-meter-long tube section of SBRA has five instrumentation ports that are equally spaced and constant bore of 38.1 mm. The 2-m-long RTRA shell tube has a 76.2-mm-bore and 114-mm-O.D. Each tube of the test section can be filled with different gases that are isolated by installing Mylar diaphragms at its joints. This was routinely done in experiments that required more than one stage, e.g., the four-stage experiment in Figure 2.3. In this project, only the second 2-m tube of the test section was replaced with a RTRA tube. The first 2-m of the test section was evacuated and it acted as a smooth bore extension to the launch gun. The schematic of the entire ram accelerator system can be seen in Figure 3.2. The configuration of the entire test section is documented in Table 3.1.

Section Number	Length (m)	Status
1 (Smooth-bore tube)	2	Evacuated
2 (RTRA)	2	Filled with propellant
3 (Smooth-bore tube)	12	Evacuated

Table 3. 1: Test section configuration

Each instrumentation station has 2 to 4 equidistant instrumentation ports oriented circumferentially. The ports are compatible with standard piezoelectric pressure transducers and electromagnetic (EM) sensors. Each station was equipped with one pressure transducer and one electromagnetic sensor. The pressure transducer was to collect the pressure at that particular station as the projectile passed by. The EM sensor would interact with the neodymium magnet inserted in the projectile cavity such that the arrival time of the projectile would be collected. Both measurement devices had the ability to capture the location of the projectile as it blasted through the system. However, past experiments showed that EM sensors tended to provide a much cleaner location measurement

than the pressure transducer did. A National Instruments PXIc-1071 bus was used in this experiment. The 32-channel PXIc-1071 bus collected data from the PCB and EM sensors at a frequency of 1.25 MHz. The pressure arrival times and the pressure at the tube inner wall was measure by the PCB sensors, while the arrival time of the neodymium magnet in the projectile was captured by the EM sensors. The instrumentation port distribution in this project is documented in Table 3.2 (stations 6-10 were in the RTRA).

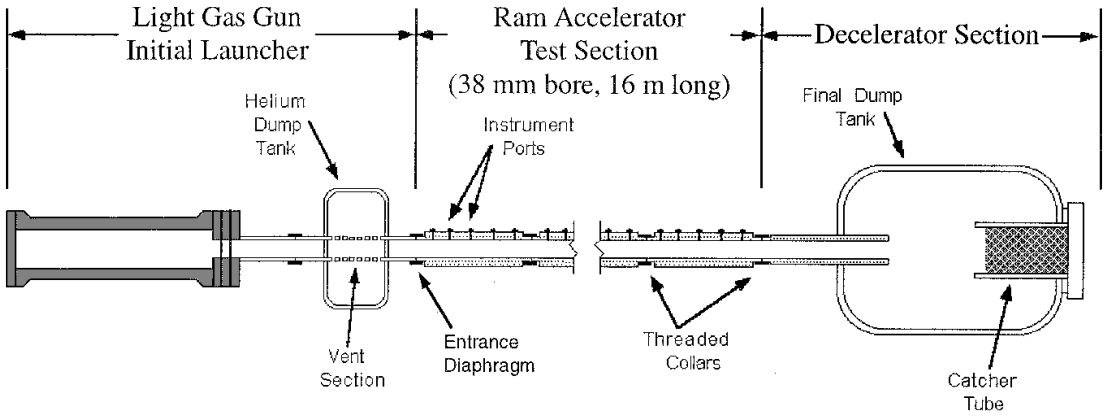

Figure 3. 2: Schematic of the ram accelerator in University of Washington

Station Number	Distance from Test Section Entrance (mm)	EM Sensor	Pressure Sensor
1 (1st instrument station)	200	Yes	Yes
3	1000	Yes	Yes
5	1800	Yes	Yes
6 (1st RTRA station)	**2107**	**Yes**	**Yes**
7	**2464**	**Yes**	**Yes**
8	**2831**	**Yes**	**Yes**
9	**3188**	**Yes**	**Yes**
10 (Last RTRA station)	**3545**	**Yes**	**No**
11 (evacuated tube)	3852	No	Yes
12	4252	No	Yes
13	4652	Yes	Yes
14	5052	No	Yes
15	5452	Yes	Yes
16	5852	Yes	Yes

Table 3. 2: Instrumentation ports location and sensors (red stations in RTRA)

Gas Handling

The ram accelerator facility used Brooks Instrument Mass Flow Controllers (MFCs) to control the molar ratios of the gas mixtures (fuel, oxidizer and diluent if needed). The gases were first mixed inside the tubing before they were allowed to enter the actual test section segment. The calibration of the MFCs was based on the time derivative of the ideal gas equation.

$$\frac{d}{dt}(PV = nR_uT) \quad (3.1)$$

where *V* is the filled volume of the test section, *T* is the temperature, *P* is the fill pressure, *n* is the molar count and R_u is the universal gas constant. In this calibration method, it is assumed that the volume and pressure are constant. Rearrange the equation above one can get:

$$\frac{dn}{dt} = \frac{dP}{dt}\left(\frac{V}{R_uT}\right) \quad (3.2)$$

One of the 2-meter-long tube section was isolated from the rest of the ram accelerator with Mylar diaphragms during the calibration. The section under calibration was pressurized and the pressure was monitored via LabView while calculating the $\frac{dP}{dt}$ ratio for a given MFC flow percentage (set point). A specific $\frac{dP}{dt}$ ratio was needed for a given gas mixture molar ratio and the result was correlated to the MFC flow percentage point. The calibration points were then linearly interpolated or extrapolated to calculate the flow percentage for a given gas mixture molar ratio.

In a typical ram accelerator experiment, the gas handling procedure is the following:

- Isolate active ram accelerator sections (filled with propellants and oxidizer) from the rest of the system

- Vacuum the rest of the launch system via two vacuum pumps
- Fill up the active ram accelerator sections with nitrogen to purge any gas residue from the previous experiment
- Set fuel and oxidizer percentages in MFC
- Turn on the supplies of fuel and oxidizer (valve downstream pressure = 500 psi) and let the gas mixture flow through the dump line until the flow is stabilized
- Close dump line and turn on fill line to fill the active ram accelerator sections with gas mixture
- Pump helium to the breech and inter-diaphragm to around 2000 psi simultaneously
- Stop pumping helium to inter-diaphragm when the system reaches around 2000 psi but continue pumping helium to the breech until the diaphragms rupture (around 4000 psi)
- Activate the vacuum pumps to vacuum combustion remaining in the system
- Open the dump line

Railed-Tube Design

Currently, the SBRA and finned projectile are utilized to accomplish high muzzle velocity in the ram accelerator. However, this solution is costly. Finned projectile manufacturing is much more complicated and expensive than that of an axis-symmetric projectile. This drawback would be exacerbated if large amount of projectiles are to be launched on a daily basis. Thus, an alternative solution is required to minimize future ram accelerator launch cost.

Although the manufacturing cost of the railed-tube insert is expensive and labor intensive, the railed-tube insert allows the use of relatively simple and inexpensive axis-symmetric projectiles while, theoretically, retaining a similar if not identical performance of the SBRA (with finned

projectiles). The railed-tube design in this project was only meant for risk reduction testing and proof-of-concept to guide design of a more robust, higher pressure rated RTRA.

Reason number one is that there are minimal previous rail designs in the ram accelerator world [13,14]. Hence, the current rail design is a prototype. The rails inside the shell tube with an ID of 3.0” and OD of 4.5” are floating due to the mounting stand offs. It is unclear at this point how the floating rails will affect the flow field as well as whether this will have performance penalty compared to a smooth-bore TCRA that has no structure inside the tube to obstruct the flow.

Reason number two is there was a very tight time constraint during the design, manufacturing and experiment process. The railed-tube system consists of four 2-meter-long rails and 8 centering rings. The rails guide the projectile while the centering rings keep the rails in place. As seen from the Figure 3.3 and Figure 3.4, the final version of rail has a very simple rectangular T shape to minimize the machining difficulty, thus reducing the total machine time to 80 hours roughly. This translated to about 4-weeks machining time in the UW A&A Machine Shop.

Most finned projectiles in the previous experiments and projects had a 0.100”-wide fin. Because rail acts as the fin for projectile stabilization, the dimension of the rail structure in contact with the projectile was designed to be the same as 0.100”. This will allow the rail system to have a closer resemblance to the smooth bore system. Increasing the thickness of the rail in contact with the projectile will lower the unstart upper Mach number of the system because the shock-train at the shoulder of the projectile will not be able to relive if the thickness of the rail is too large. The corners of the rail structure were chamfered to simplify the machining process.

There are six equally spaced notches on each 2-meter-long rail, where they are mounted to the centering rings, and each notch has a 4-40 UNC tap hole. The notches are equally spaced so that

there will be one set of instrumentation port between two notches and centering rings. This can minimize the interference of the centering rings to the pressure transducers. To guarantee enough clearance for the projectile with a 1.5" diameter to fly through at a supersonic speed, the height of the rail structure has a tight tolerance of ±0.003".

Experiments in the smooth-bore TCRA with finned projectile in the past indicates that a diameter ratio of less than 0.55 would lead to 'unstart' in energetic propellants. Diameter ratio is the following:

$$DR = \frac{D_p}{D_b} \quad (3.3)$$

where D_p is the diameter of the projectile while D_b is the diameter of the bore. In baffled tube and railed tube, there is no diameter ratio due to the non-uniform structures. Thus, the effective area ratio is introduce.

$$AR = \frac{A_p}{A_{flow}} \quad (3.4)$$

Note that the effective diameter ratio is the square root of Equation 3.4. Data show that ram accelerator operation with an effective diameter ratio at around 0.6 to 0.85 was feasible. Therefore, achieving a desired effective and functional area ratio is the most important factor during the design process of the rail prototype. The final version of the rail design has an effective diameter ratio of 0.625.

Figure 3. 3: Rails of the prototype RTRA

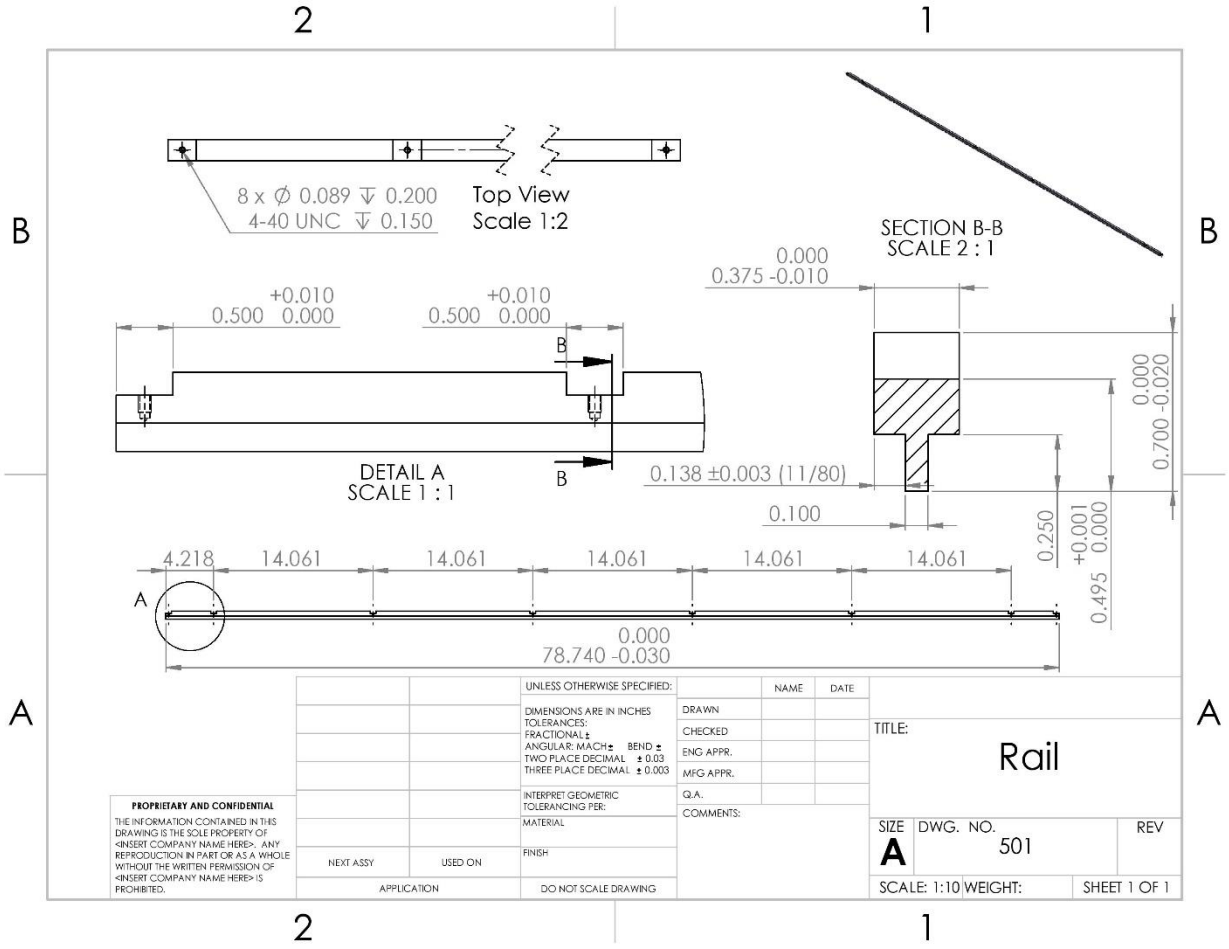

Figure 3. 4: Rail design part drawing

Centering Ring Design

The centering rings are to hold the rail in place such that the projectile will not be obstructed through the tube. As seen from Figure 3.6, the centering ring has an OD (outer diameter) of 2.998” to 2.996”. This allows the centering rings to be slide into the tube with a 3” bore. The ID of the centering ring was designed to be 2”, which led to a diameter ratio of 0.75. There are 4 quarter-inch-deep notches on the inner surface of each centering ring and each notch has a 0.129” through clearance hole. The corners of the notches had circular drill holes in order to minimize machining time. The thickness of the centering ring was determined to be 0.5”, which is twice the thickness

of each baffle section (both normal and slanted). Previous baffled tube analysis and experiments indicated that 0.5” thickness can avoid local baffle buckling (Figure 3.5). Due to the time constraint, the centering ring design shared some similarities with the baffles to guarantee structure strength.

The centering rings at each end of the 2-meter-long railed tube sit against the flanges. This effectively locks the entire rail structure to prevent sliding motion. An ideal railed-tube ram accelerator design should not contain centering ring structure. The centering rings in this prototype will cause wave reflections whose effects on operation are expected to be negligible, but subject to verification. Since the gap between two centering rings is more than 2.5 projectile-caliber apart, it is speculated that the flow obstruction due to the centering rings will not prevent the system from running in a thermally choked propulsive mode. If this project proves that railed-tube ram accelerator can produce similar or identical thrust performance compared to the smooth bore TCRA, the future railed-tube design will have more aerodynamically optimized shape with the aid from CFD analysis, and the rail structure will be mounted directly on the bore instead of utilizing centering rings.

Figure 3. 5: Baffle local buckling

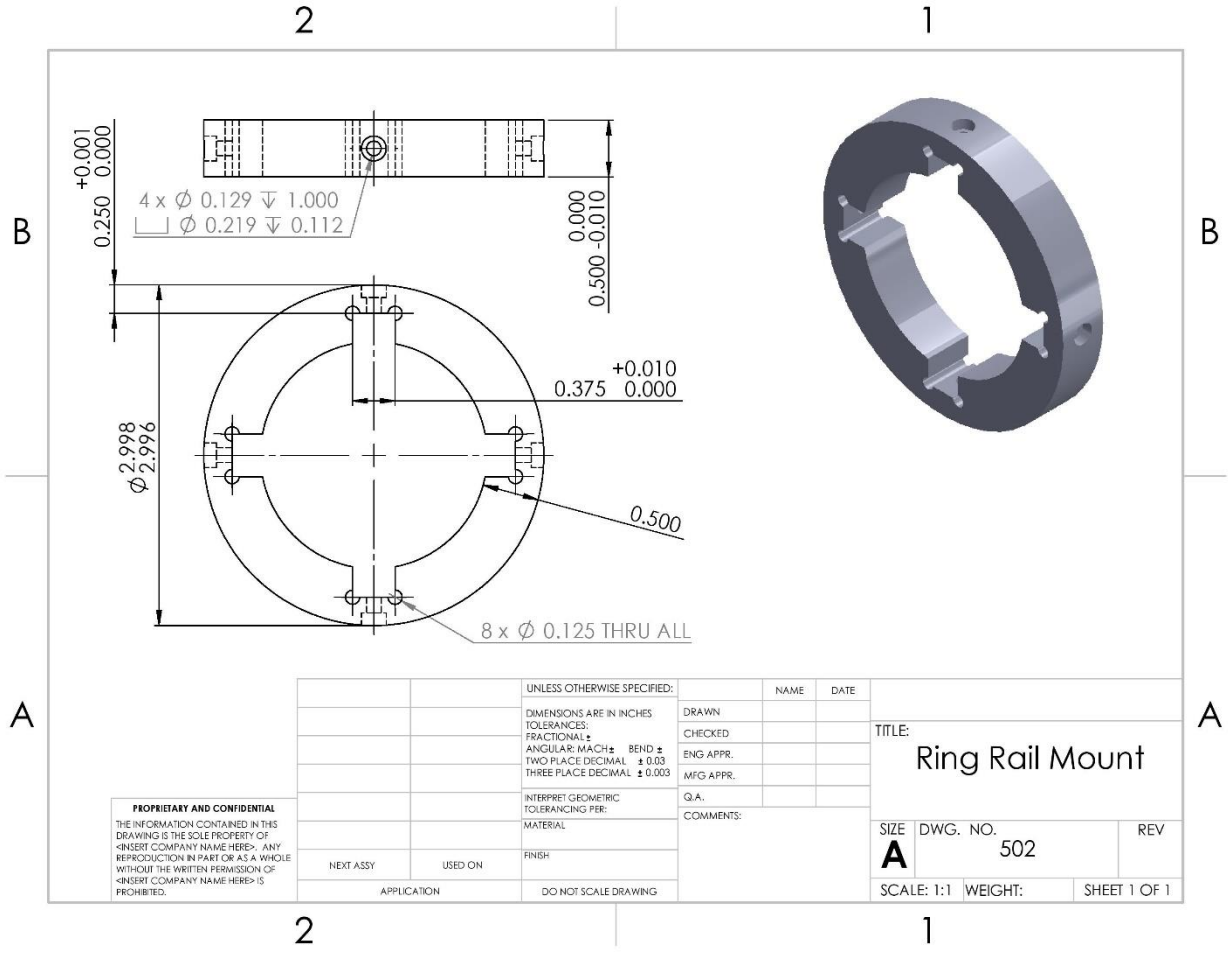

Figure 3. 6: Centering ring part drawing

Figure 3. 7: Shell tube with 3” bore and its railed-tube insert

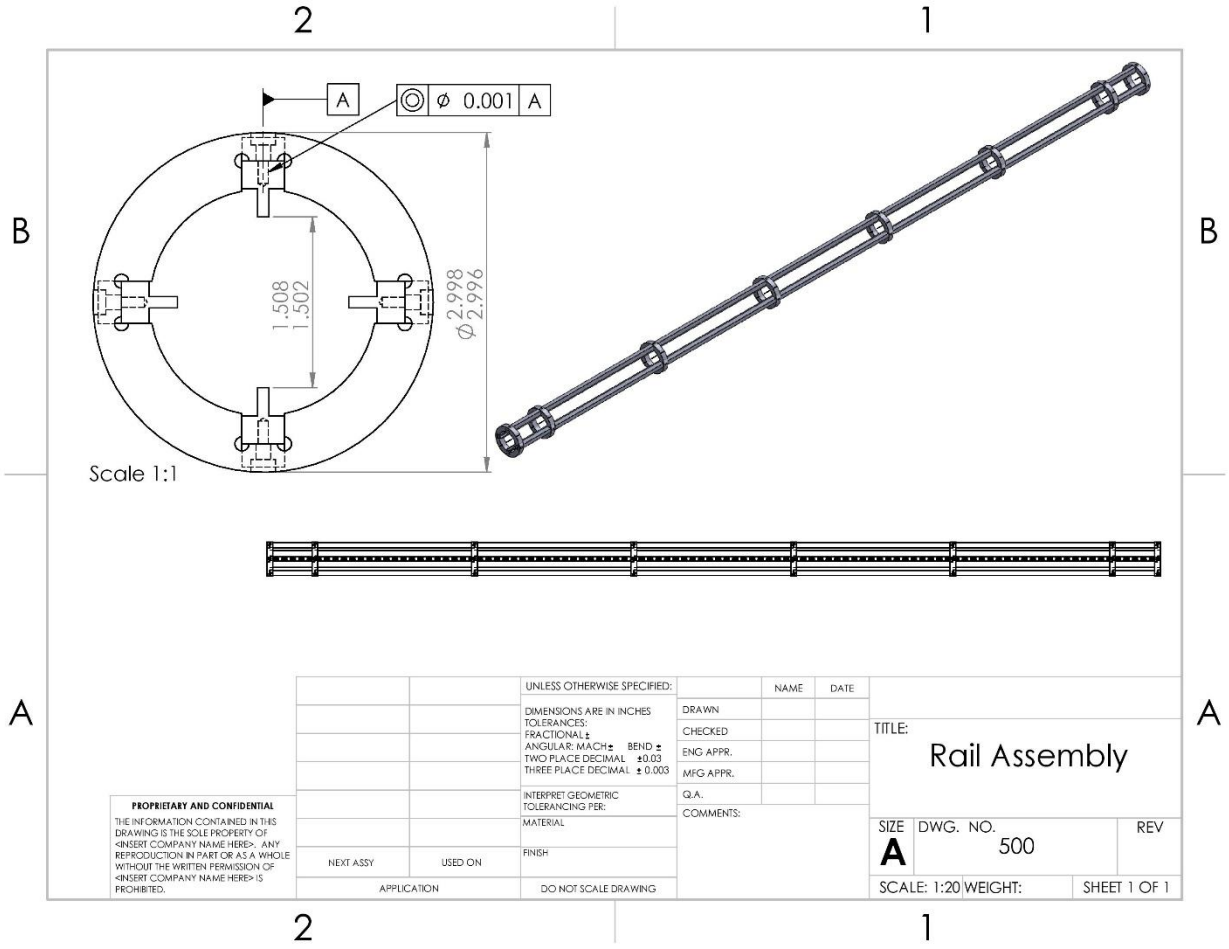

Figure 3. 8: Railed-Tube insert Assembly Part Drawing

Projectile & Piston Configuration

For the RTRA experiments presented in this paper used axis-symmetric projectiles with a piston obturator (Figure 3.10). The piston was 1.474” in diameter, 1.25” in length, and had a mass range of 22-24 grams. It occludes the expanding light gas gun propellant (helium) that propels the projectile to desired entrance velocity to the active ram accelerator section. Typical ram accelerator entrance velocities for this series of experiments were 1000 m/s to 1100 m/s with light gas gun pressure at around 5000 psi.

The projectile had to be glued on the piston and the contact surface must be reasonably flat. Any non-even contact surface would result to launch failure because the piston would slam onto the base of the projectile at the moment the diaphragm set in the gas gun burst instead of pushing it, which would smash the projectile into pieces before it entered the ram accelerator section. The in-depth analysis of the functionality and importance of the piston can be found in [15].

The projectile (Figure 3.9) was made of polycarbonate to minimize weight and cost. Since the experiments were conducted at relatively low pressure, the strength of the projectile was not a critical factor, allowing the use of polycarbonate. The projectile in this project was initially designed for the BTRA so that it had a slightly smaller throat diameter than it should for the RTRA. Future RTRA experiments would be conducted with projectiles properly sized for the rail design. The projectile had a cavity of 1.74" at the base with a tap hole of ½-13 thread to store a 0.258-inch-long neodymium plug magnet, which allowed the EM probes to track the location of the projectile during the experiments. The remainder of the cavity was filled with threaded plastic spacer/stud. The projectile had a 15° (half angle) nose cone and its tail was tapered at 12°. The throat diameter of the projectile and the current rail structure design gave an overall effective diameter ratio of 0.625 between two adjacent centering rings. The length of the projectile shoulder was designed to be 2.326" due to the length of each baffled insert because the current projectile design was optimize for the BTRA.

In order to allow the baffled insert in a BTRA to act as a one-way valve, the projectile shoulder had to be at least 1.5 times the length of each baffled insert. Maximum thrust is achieved with an optimal shoulder-baffle gap, which requires a somewhat smaller projectile diameter as reported in [9]. Because of its smaller diameter, the current projectile was not able to fly in a straight line in the RTRA. Instead, the projectile would bounce between the rails or grind its way through. The

could be one of the reasons why with the current RTRA and projectile design the propellant was difficult to ignite, which would be discuss later on this paper. Future revision on the current projectile design would optimize the throat diameter and its length for better thrust performance and more consistent propellant ignition in the RTRA.

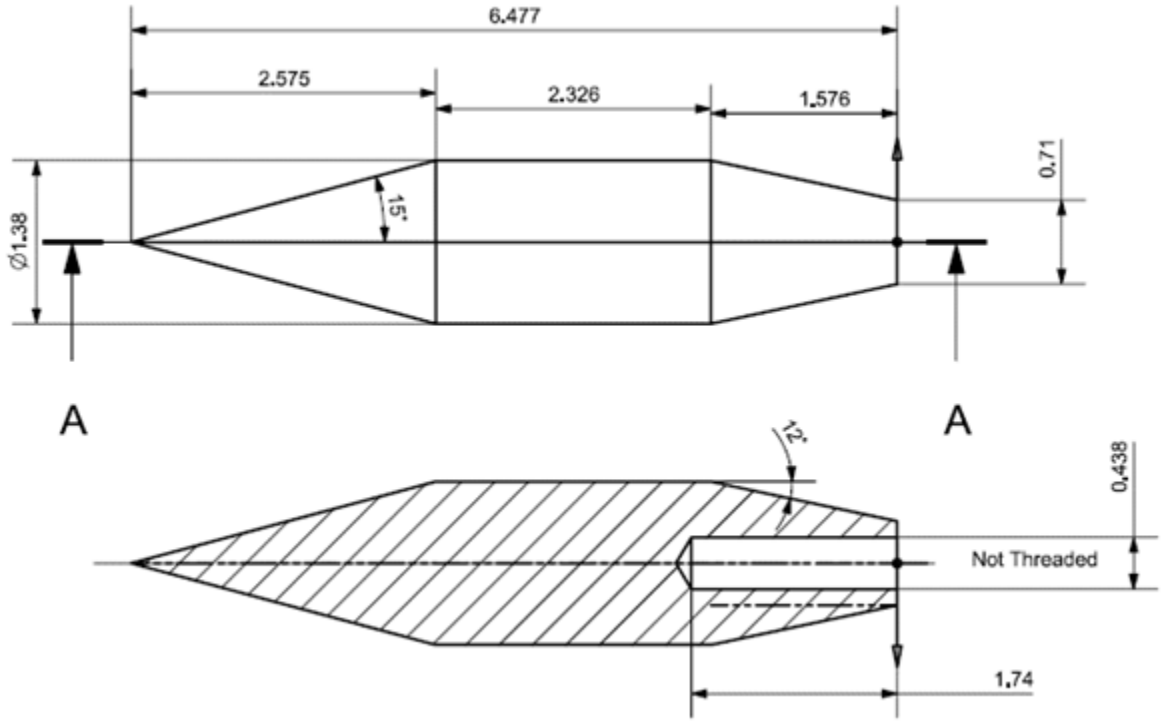

Figure 3. 9: Axis-symmetric projectile part drawing

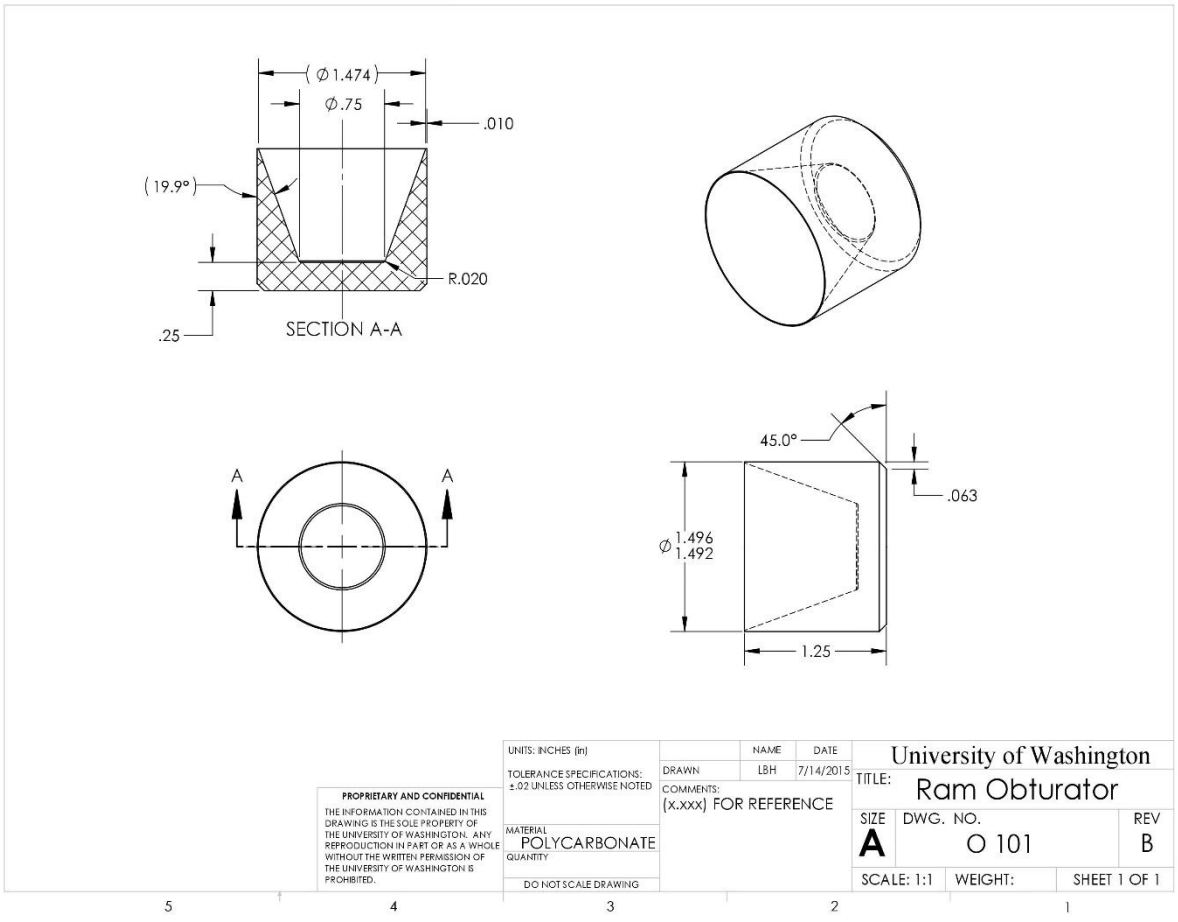

Figure 3. 10: Obturator (Piston) part drawing

Figure 3. 11: Lexan projectile and piston for the prototype RTRA

RTRA Experimental Procedure

The experiment of RTRA required special attention because high pressure combustible and inert gases were used. The experimental procedures of this project were the following (some were already mentioned in the *Gas Handling*):

1. Prepare projectile by loading it with neodymium magnet and plugging the rest of the cavity with plastic threaded spacer/stud, as well as flattening the projectile base with a bell sander.
2. Weigh the projectile and the piston on a balance scale individually, as well as the total weight of both.
3. Glue the projectile (its base) to the piston with few drops of super glue.
4. Load the combination into the launch tube downstream of the helium gas gun.

5. Install aluminum diaphragms on the breech, with 4 downstream and 3 upstream (relative to the recoil bumper) based on the breech pressure.
6. Record diaphragm configuration and sealed the helium gas gun.
7. Install the recoil bumper.
8. Isolate the active ram accelerator section with 0.014”-thick Mylar diaphragms and sealed the ram accelerator section.
9. Pack catcher tube at the final dump tank with an aluminum block, multiple diaphragms and carpet rolls and sealed the final dump tank.
10. Pressurize the ram accelerator section with N_2 to check for leak.
11. Confirm electrical continuity across the instrumentation suite and tested data collection triggering mechanism.
12. Vacuum the entire system with both vacuum pumps and check for leak of the entire system.
13. Turn on gas supply in the gas bunker and started filling propellant and oxidizer into the ram accelerator after the mass flow controller stabilized.
14. Check helium bottle pressure and calculated how much helium was consumed based on the reading from the previous shot.
15. Start the pump to pump helium into both breech and gas gun simultaneously; stop pumping helium into breech once desired breech pressure was obtained but continue this process in the gas gun.
16. Check if the data acquisition program was triggered; restart the ‘run’ if it was triggered.
17. Keep pumping helium until the shot was completed.
18. Shut off the pump and turn off helium bottles.

19. Vacuum the entire system to prevent remaining combustion products from propagating into the lab space.
20. Shut off fuel and oxidizer supply in the gas bunker.
21. Open the ram accelerator section (its joints) to remove broken Mylar diaphragms and opened the gas gun breech to remove broken aluminum diaphragms.
22. Clean up sealing surfaces of the ram accelerator section.

Upon launch the projectile passed the first EM sensor and this triggered the data collection system to save data that occurred within a specified time span. The EM sensors in the system tracked the projectile all the way to where the last EM sensor was placed. The pressure transducers tracked the wave activity in the system (shock especially). For a successful operation, the projectile position data from the EM sensors should coincide with the shock system data from the pressure probe.

CHAPTER 4: EXPERIMANTAL RESULTS AND DISCUSSION

In this chapter, the raw data collection and processing will be discussed as well as the procedure to analyze the data. Collection of raw data requires the use of LabVIEW and the processing of the data requires the use of MATLAB. The pressure and EM data in the initial RTRA experiments will be analyzed. The axis-symmetric projectile performance in the RTRA and its comparison to the TCRA theoretical thrust performance will be discussed in this chapter.

Collection and Processing of Raw Experimental Data

In the UW ram accelerator facility, position and pressure raw data were collected with EM and PCB sensors across 32 channels at 1.25 MHz. The EM sensor record the location of the projectile by interacting with the magnet installed inside the cavity of the projectile. The PCB record the pressure wave magnitude and its time of arrival. To maximize the available channels for PCB, the EM sensors were grouped in six strings and their signals amplified with multiplexers. Each PCB, on the other hand, populated one channel and was individual amplified. The National Instruments PXIc-1701 data acquisition system and LabVIEW converted signals into an *.lvm file. Previous student researchers had developed a MATLAB script to read the *.lvm files, and plot the pressure and EM signals.

The velocity and acceleration of the projectile were determined by the EM signals for time-of-passage. One can construct the velocity-distance/acceleration-distance diagrams based on the EM signals. While the pressure wave signal could do the same thing, it could also determine the wave activity from which one could estimate the gasdynamics of each shot. The pressure data was useful in determining whether an unstart, wave fall-off, broken projectile/piston or successful operation

occurred at a given station in the ram accelerator. Moreover, by combining the time and location data of both sensors, one could determine the relative position of a shock or wave system to the projectile.

Railed-Tube Ram Accelerator Data Analysis

Because RTRA system for TCRA has not been significantly explored and there was no theory guidance, the primary objective of this thesis project was to determine if a successful ram accelerator start and subsequent acceleration can be establish under any conditions. The performance characteristic of the RTRA was speculated to be the same as the smooth-bore TCRA, if and only if the system operated at the thermally-choked propulsive mode.

The initial prototype RTRA tests had two experiment parameters: fuel equivalence ratio and fill pressure. A low speed start experiment was also conducted in the RTRA by accident. All propellant mixtures in this thesis project were methane/air. Four equivalence ratios were used in this series of tests and their properties were documented in Table 4.2. Although other propellant mixtures were viable options for the RTRA and the SBRA, methane/air mixture was chosen for this experiment because it was commercially abundant and inexpensive. Table 4.1 shows the propellant mixture, projectile entrance velocity and exit velocity, projectile mass, ram accelerator filled pressure, entrance Mach number during the experiment, non-dimensional thrust based on the entrance Mach number. For the detail of the theoretical non-dimensional heat release as a function of Mach number of the mixtures used in this project, please refer to Figure 4.15.

Shot Ref#	Propellant	U_{in} (m/s)	U_{out} (m/s)	m_p (g)	P (psig)	M_{in}	I_{exp}
HS2079	2.5 CH_4 + 9.52 Air	1050	1064	122	144	2.91	~0
HS2080	2.0 CH_4 + 9.52 Air	1043	1055	122	162	2.91	~0
HS2081	1.5 CH_4 + 9.52 Air	1036	1036	123	154	2.91	0
HS2082	1.0 CH_4 + 9.52 Air	778	778	122	160	2.21	0
HS2083	1.0 CH_4 + 9.52 Air	1062	1092	122	149	3.01	0.40
HS2084	1.0 CH_4 + 9.52 Air	887	613	122	225	2.52	N/A
HS2085	1.0 CH_4 + 9.52 Air	1030	1118	122	225	2.92	0.82

Table 4. 1: Initial RTRA experiment result

Propellant	Φ	Q_{cj}	V_{cj} (m/s)	a_1 (m/s)
2.5 CH_4 + 9.52 Air	2.5	4.42	1650	361
2.0 CH_4 + 9.52 Air	2.0	5.58	1740	358
1.5 CH_4 + 9.52 Air	1.5	6.88	1820	356
1.0 CH_4 + 9.52 Air	1.0	7.80	1850	353

Table 4. 2: Propellants properties

In this project, all experiments were able to accomplish gasdynamic start, except HS2084 where the test had failed due to piston blow-by. When a projectile started gasdynamically, it was able to maintain supersonic flow at its throat region. The projectile nose cone was able to remain ahead of any shock/wave system across the entire RTRA. Pressure profiles from Figure 4.3 to Figure 4.6 prove that the projectiles were able to achieve gasdynamic start. The areas of interest in these pressure profiles were the lead wave, reflection off the shoulder, and pressure wave activity near base of projectile.

The lead wave, in all of these tests on the RTRA, was the conical shock generated by the projectile nose cone. The lead wave was identified as the first pressure spike in a pressure signal plot. The data cursors in the pressure plots were the time of arrival from the EM sensor at that particular station, which demonstrated the relative location of the projectile with respect to the conical shock. As mentioned earlier in this paper, the neodymium magnet was install at the base of the projectile, with its center located 15.6 mm from the projectile base (Figure 3.9). Therefore, the EM signal

would not be at the beginning of pressure spike; instead, it would be in a position shortly after the time of arrival of the lead wave. One can verify the location of the projectile nose cone relative to the lead wave location. For example, in HS2080, the average velocity was around 1050 m/s, which corresponded to 1.05 m travel distance per millisecond. At the station 6, the lead wave started at 10.010 ms while the EM arrival time was at 10.055 ms. There was a time delta of 45 μs and with the average velocity across the RTRA, one could easily calculated the distance of travel corresponding to this time delta to be ~47 mm, which was roughly the distance between point where the conical shock generated by the nose cone impacts the wall and the magnet. However, this point was not the tip of the nose cone because the conical shock had an angle and the pressure transducer only record the pressure rise from the shock.

The shock angle can only be estimated. It cannot be accurately calculated because of the uncertainty of the velocity data (~ ±20m/s). The distance between the magnet and the nose cone of the projectile (D_1 = 12.02 mm) was known based on the design of the projectile. The distance between the magnet and the shock location (D_2) for a given station could be calculated based on the time of arrival delta between the EM signal and the pressure signal (lead wave or first pressure spike in the plot). Then, the distance between the nose cone and the shock location (ΔX) could be calculated by subtracting the D_2 from the D_1. If ΔY (3.81 mm) was the distance between the tip of the nose cone to the tube wall, the conical shock angle θ could be estimated by $\theta = tan^{-1}(\frac{\Delta Y}{\Delta X})$. For example, in station 6 of HS2080, D_2 was calculated to be 47mm, resulting to ΔX = 8.21 mm. This corresponded to a conical shock angle θ of 24.9°. The schematic of the shock reflection between the projectile and the tube wall is shown in Figure 4.1.

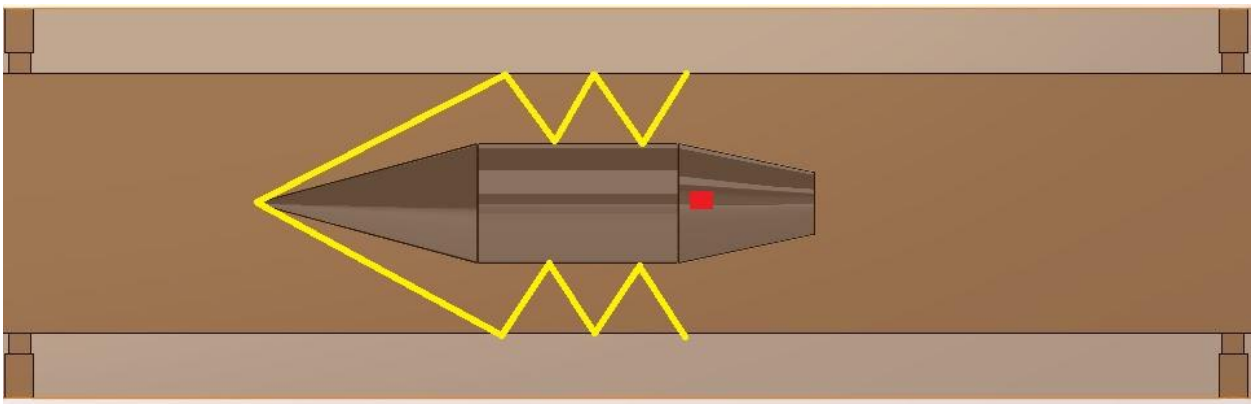

Figure 4. 1: RTRA shock reflection schematic

The pressure profiles from station 6 through 9 in all successful test on the prototype RTRA combining the EM signals demonstrated the same information shown in the HS2080 pressure profiles. Hence, one can confidently conclude that all experiments where the projectile is ahead of waves in launch tube when it enters the RTRA accomplished gasdynamic start. Note that the pressure signal of HS2080 at station 8 had artifact so that the pressure signal at station 8 of HS2081 was provided instead.

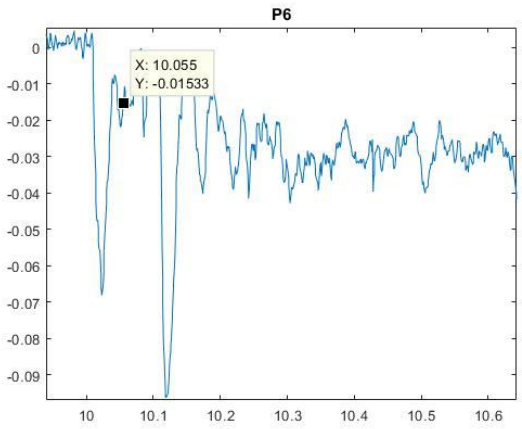

Figure 4. 2: HS2080 pressure plot at station 6

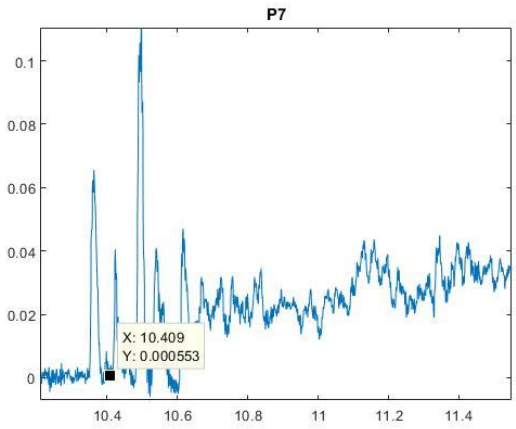

Figure 4. 3: HS2080 pressure plot at station 7

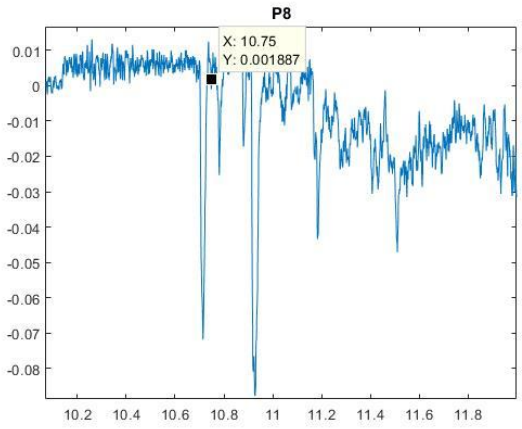

Figure 4. 4: Pressure plot of HS2081 at station 8

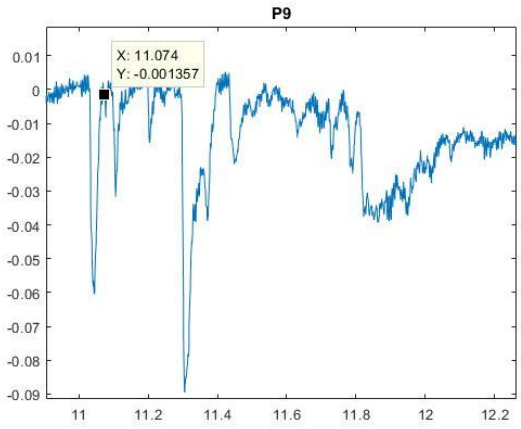

Figure 4. 5: Pressure plot of HS2080 at station 9

The experiment on RTRA started with a 'cold' mixture – fuel rich mixture (additional methane) with N_2 in the air as diluent to cool down the combustion. The first propellant used during the investigation of the RTRA operation envelope and performance was the $2.5CH_4 + 9.52$Air mixture. This mixture had trouble to initiate combustion in the SBRA system and was believed to be unable to operate in the RTRA as well. The result of HS2079 proved this assumption correct. According to the EM data, the projectile did not accelerate as it passed through the RTRA. Instead, it coasted through the 2-m-long test section without losing much, if any velocity. This was a clear indication of a wave fall off scenario because this propellant contained too much diluent for the SBRA and RTRA system. Thus, this mixture was too cold for the current projectile geometry and entrance Mach number, and thus this propellant was not ignited in this experiment. The projectile was still able to maintain, with no obvious combustion activity, the same speed indicated that velocity multiplication might had played a role, as explained below.

In short, once the projectile and piston enter the RTRA, the piston, with much larger area perpendicular to the tube bore, will push the gas and a shock toward the projectile. The projectile

will briefly be accelerated by the high-pressure region generated by the piston until the velocity of the piston decays significant enough, i.e., the piston and projectile are far enough apart. If the piston has an infinite mass, it will not slow down at all in the test section and eventually the shock generated by the piston will overtake the projectile, causing unstart. If the piston is too light-weighted, it will slow down rapidly as it enters the test section and the projectile may not be affected by the piston gasdynamic effect at all. This is called the velocity multiplication.

The pressure signal at station 6 in HS2079 (Figure 4.6) supported the argument that there was no obvious combustion activity occurred in the test. The first pressure spike was followed by two other pressure spikes. It was believed that the subsequent two pressures signals were the shock reflections between the rail or tube and the projectile body. Normally, the reflection should have lower magnitude than the lead wave. However, in this project, the projectile only had a throat diameter of 1.380", which allowed it to cant as it traveled through the RTRA. This could potentially affect the strength of the reflected waves.

One can also determine whether a combustion occurred based on the magnitude of the pressure wave. Figure 4.7 shows a typical pressure plot with propellant combustion in the BTRA. Note that the BTRA pressure plot does not have EM signal because, in the BTRA, EM sensor was not able to produce a clean signal due to the interference of baffles. The first drop from the pressure plot was the conical shock at the nose cone of the projectile. Then the pressure recovered slightly shortly before another big spike with a magnitude greater than any other signal spike in the plot. This pressure spike was a clear indication of combustion as it occurred shortly after the nose cone conical shock. If one carefully observed the time delta between these two points, one could calculate the physical length between them with the projectile velocity data (from the EM signals) at that station. One thing worth mentioning is that when the ram accelerator operates in the

thermally choked propulsive mode, the combustion does not necessarily occur right at the base of the projectile. Hence, the calculated distance does not have to be exactly one-projectile length. In Figure 4.3, the magnitude of the conical shock (lead wave) was similar to those of the subsequent pressure spikes, indicating that no obvious combustion had occurred in this experiment.

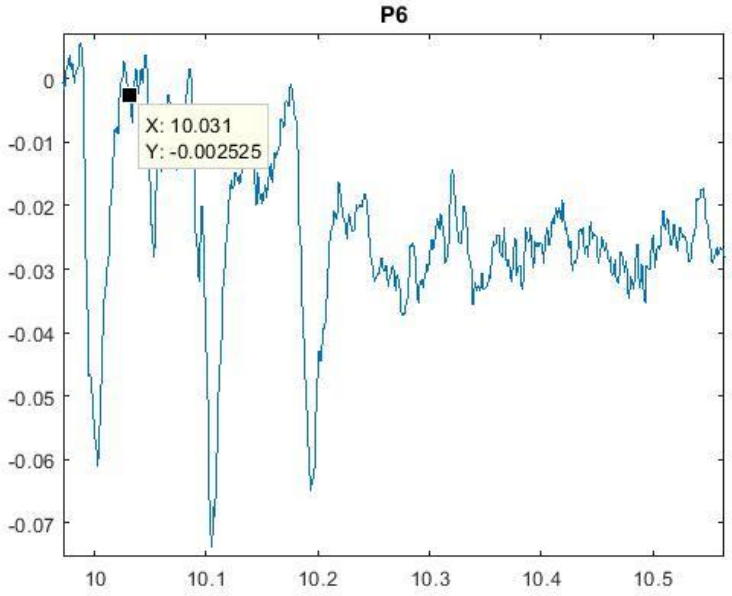

Figure 4. 6: HS2079 pressure plot at station 6

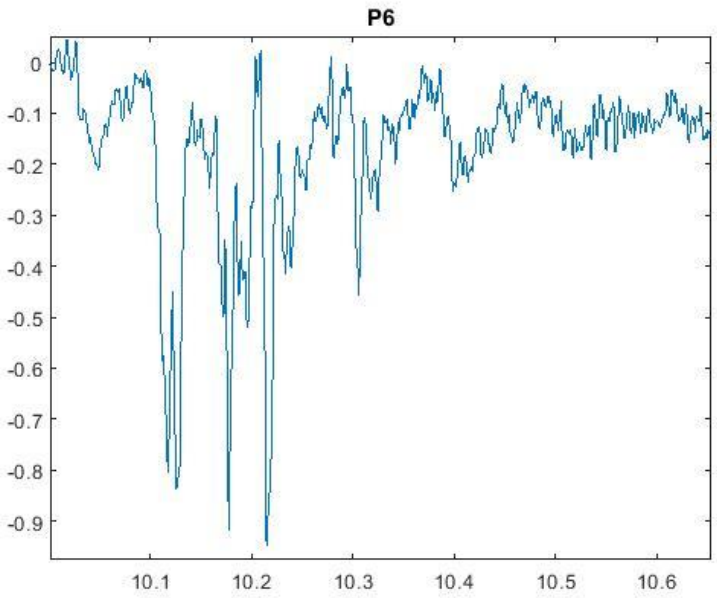

Figure 4. 7: BTRA pressure plot with combustion activity (pressure signal at station 6 in HS2078)

HS2079 served as a base line for the rest of the RTRA experiments. It was clear that the HS2079 propellant mixture was simply not energetic enough to enable ignition. Thus, in HS2080 and HS2081, the amount of CH_4 was reduced to 2.0 and 1.5, respectively. In a methane/air mixture, additional methane served as a diluent to absorb the heat from the chemical reaction and methane is very good at trapping heat. To make the mixture hotter, one must reduce the amount of methane until the stoichiometric methane/oxygen reaction ratio, where the mixture would be at its hottest. The results of the HS2080 and HS2081 were very similar to that of HS2079 with no obvious sign of combustion event. This indicated that the mixtures of $2.0CH_4$ + 9.52Air and $1.5CH_4$ + 9.52Air were still not energetic enough to initiate combustion.

ISL conducted few experiments on RTRA in the past and Figure 4.8 shows a pressure profile of the RTRA in ISL. It is interesting to see that the pressure profiles from both systems share some

similarity – with two pressure spikes following the lead wave. However, the rails of the RTRA in ISL were machined directly into the tube wall while the RTRA in UW had 'floating' rail design.

The railed-tube insert in the prototype RTRA was removed from the shell tube for physical inspection after HS2081. No physical indication of combustion was observed during the inspection, which further proved the speculation to be correct – i.e., no combustion occurred in HS2079, HS2080 and HS2081. The propellant mixtures in these two experiments were simply not hot enough for ignition at the current prototype RTRA, projectile design, entrance Mach number, and fill pressure (~11 atm).

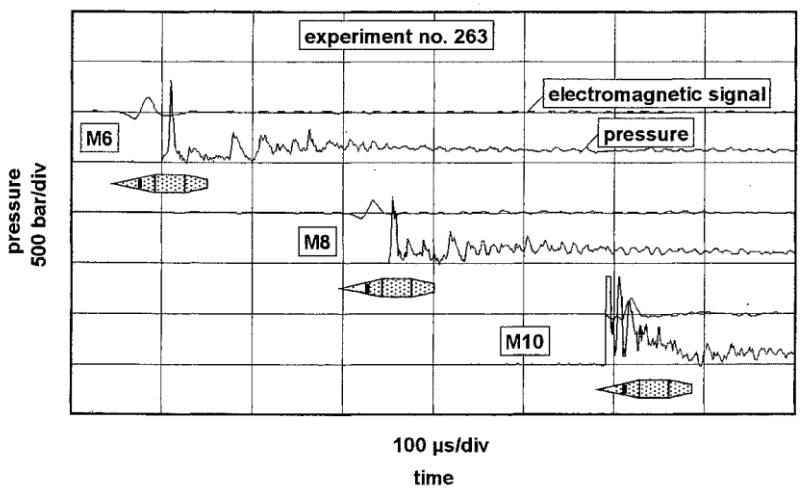

Figure 4. 8: Pressure profile of firing no. 263 in ISL

Positive projectile acceleration was first observed in HS2083, where the methane content in the propellant mixture was further reduced to 1.0 CH_4 + 9.52 Air. Note that 1.0 CH_4 + 9.52 Air is equivalent to 1.0 CH_4 + 2.0 O_2 + 7.52 N_2, which is the stoichiometric methane/air propellant. In this the experiment, the projectile was not only able to maintain its entrance velocity but also gained roughly 30 m/s based on the EM data. This velocity gain measurement exceeded the uncertainty of the velocity data (±20m/s), indicating that the system could have a ram accelerator

start, i.e., combustion. From the Figure 4.9 and 4.10, one can see that the peak magnitude of the pressure signals after the lead wave was at around 0.15 to 0.2 millivolt. Although the pressure probe was not calibrated in this series of experiments, it still had a conversion of 1 mV = 10 psi. This translated to a pressure of around 1500 psi in station 6 (after 11 ms) and almost 2000 psi in the station 7. Since the filled pressure of this experiment (HS2083) was 150 psi, it was very likely that combustion activity occurred in this test.

To further verify this speculation, the railed-tube insert was removed again for inspection. Combustion remains were detected in the railed-tube insert and the remaining of the Mylar diaphragms, as well as the smell of combustion. From the pressure plots in Figure 4.9 and Figure 4.10, one could tell that the combustion had occurred roughly between 11 ms and 20 ms, which was behind the projectile itself.

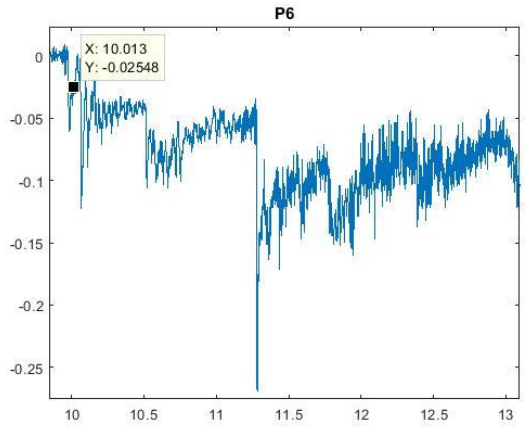

Figure 4. 9: HS2083 pressure plot at station 6

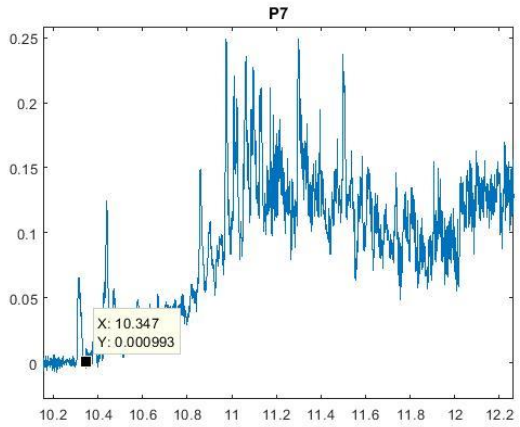

Figure 4. 10: HS2083 pressure plot at station 7

Once the mixture of 1.0 CH4 + 9.52 Air was identified as a potentially useful mixture, the filled pressure parameter was raised. In a ram accelerator, accomplishing a start does not necessarily mean high acceleration or velocity delta. In order to obtain hypersonic launch velocity in short

distances, the filled pressure of the ram accelerator must be increased dramatically if only a single stage is utilized. The filled pressure was raised to 225 psig (16 atm) in HS2085. The experiment was proven to be partially successful. The projectile obtained approximately 90 m/s velocity delta and there was very clear indications of combustion from the physical inspection on the railed-tube insert and the velocity data. Compared to HS2083 shot, the projectile was able to gain additional velocity across the RTRA, which indicated that increasing the filled pressure would proportionally increase the thrust of the projectile, thus higher velocity gain. Data shown in Figure 4.11 is characteristic of malfunctioning PCB sensor, whereas the noise on the pressure trace in Figure 4.12 is likely a wiring issue. Even though there is significant noise in the Figure 4.12 trace, the data from the lead shock was relatively clean and showed that it was ahead of the EM signal by the expected time interval. The pressure behind the projectile and presumably in the combustor zone was too noisy for easy interpretation as is, but it may be possible to clean it up with filtering.

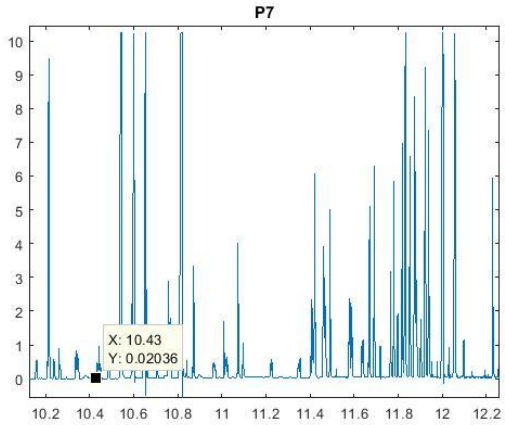

Figure 4. 11: HS2085 pressure plot at station 7

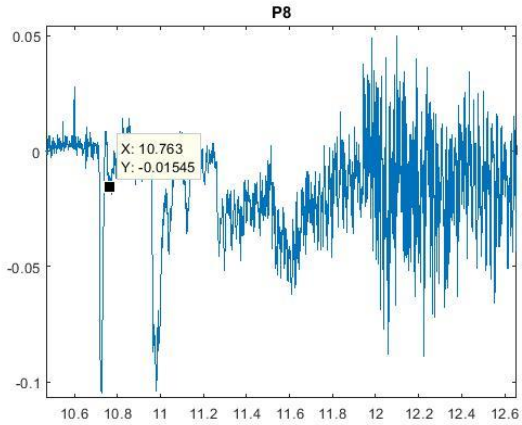

Figure 4. 12: HS2085 pressure plot at station 8

This experiment successfully accelerated a relatively massive projectile, however, it also had permanently damaged the last 20-40 cm of the railed-tube insert (Figure 4.13). It is very likely that a wave unstart occurred toward the end of the RTRA tube section, however, at this moment, it was

unclear why the railed-tube insert failed in such a manner (the railed-tube insert was completely burned and warped). The failure surface shows evidence of violent combustion (there were pieces of molten O-ring stuck on the centering ring and shell tube sealing surface), which was expected because this mixture has higher *Q* than what the SBRA system can handle. The groove on the sealing surface of the shell tube that has a stress rating of 30,000 psi and was badly damaged as part of the groove was completely ripped apart. This indicated that there must be a very strong pressure wave, most likely caused by the reflection from a diaphragm of an overdriven detonation wave, arising from the wave unstart process, being driven ahead of the projectile throat at the exit of the RTRA test section.

It was highly unlikely that the railed-tube insert was damaged before the projectile left the RTRA because the projectile was observed to gain about 90 m/s velocity in the tube. However, there was a possibility that the railed-tube insert failed before the projectile passed through. This would break the projectile into pieces and the velocity data from the EM sensors could be the velocity of the magnet instead of the actual projectile. An unstart during the operation toward the end of the RTRA test section was suspected. However, there was no meaningful pressure data at station 10 in this test to support this claim.

One thing worth mentioning is that the #4 cap screws used in the railed-tube insert and centering rings were sub-optimal. The rails were not able to be secured tightly to the centering rings with this size of screw so that the entire railed-tube insert had to be removed for inspection every two to three shots. There was a possibility that some of the bolts were loose and sheared by the high pressure region generated by the combustion in HS2085.

Figure 4. 13: RTRA railed-tube insert and shell tube failure surface

A low speed start experiment was conducted in this project by accident. The aluminum diaphragms were supposed to be scored at 1000 psi for this experiment. However, due to human error, the diaphragms were scored at 1200 psi in HS2082 instead, resulting to the diaphragm sets burst much earlier than expected. The entrance velocity was record to be 778 m/s and surprisingly the projectile was able to maintain its velocity across the RTRA. Pressure data of HS2082 did not show any trace of combustion. This was expected because the entrance velocity of the projectile was too low for an ignition, though the propellant mixture was the most energetic across all four propellants used in this project. However, the projectile was able to start gasdynamically and the velocity multiplication phenomenon was most likely the reason why the projectile was able to

maintain its entrance velocity across the RTRA. This indicated that the prototype RTRA had a promising potential for low speed start.

Note: In HS2084, piston was busted before the projectile even reached the RTRA due to improper projectile preparation. The experiment presented no information as the blowby over the piston broke the Mylar diaphragm in the RTRA before the projectile entered the test section.

In this project, positive acceleration was observed in two tests only: HS2083 and HS2085. In HS2083, the projectile was able to accelerated 30 m/s across the test section with fill pressure of 149 psig (11 atm), which corresponded to a non-dimensional thrust I_{exp} of 0.399. In HS2085, the filled pressure was raised to 225 psig (~16 atm) and the projectile was able to accelerate by ~90 m/s, corresponding to a non-dimensional thrust $I_{exp} = 0.817$. It is expected that increasing the fill pressure would increase thrust, but if the TCRA propulsive cycle was established, then the non-dimensional thrust should be the same. Compared to the predicted TCRA performance for $\Phi = 1$ propellant in Figure 4.14, both tests only achieved a fraction of the theoretical non-dimensional thrust a TCRA can accomplish. Thus, this infers that TCRA operation was not established and/or it was undergoing a starting transient process.

It is apparent from the thrust-Mach curves in Figure 4.14 that the maximum thrust for the TCRA nearly doubles over the range of propellants considered here. This cannot be verified experimentally, however, until a means to successfully start the TCRA is implemented for these test conditions. Future experiments will use a BTRA section to ignite propellant prior to it entering the RTRA.

The variation of Q with in-tube Mach is shown in Figure 4.15. A non-dimensional heat release is a property of a given propellant mixture. In this project, there were four propellant mixtures in

total: 1.0 CH_4, 1.5 CH_4, 2.0 CH_4, and 2.5 CH_4. In the TCRA theoretical performance model, both the non-dimensional thrust and heat release are a function of Mach number. In Figure 4.15, one can identify the relation between Q and Mach number, for all four propellant mixtures used in this project. The propellant mixture is more energetic as the Φ value increases, until stoichiometric ratio of $\Phi = 1.0$ is reached. The Q of the non-stoichiometric mixtures stays relatively constant as the Mach number changes, indicating that Q is not very susceptible to the change of Mach number. Whereas the Q for $\Phi = 1$ varies by over 10% over its theoretical operating Mach number range. Additionally, from Figure 4.15, one can observe that the maximum Mach number of each propellant mixture is different. The maximum Mach number in each Q – Mach number curve is the CJ Mach number of that given propellant mixture. A more energetic propellant will have a higher CJ Mach number and higher peak thrust. Because the maximum projectile velocity in the RTRA system, if the system operated in the thermally-choked propulsive mode, is limited to the CJ speed of a given propellant, the most energetic propellant ($\Phi = 1.0$) will theoretically produce the highest muzzle velocity among all four propellant mixtures in this project. And the initial experiment result proves this speculation as the most energetic propellant mixture produced the highest projectile acceleration across the RTRA.

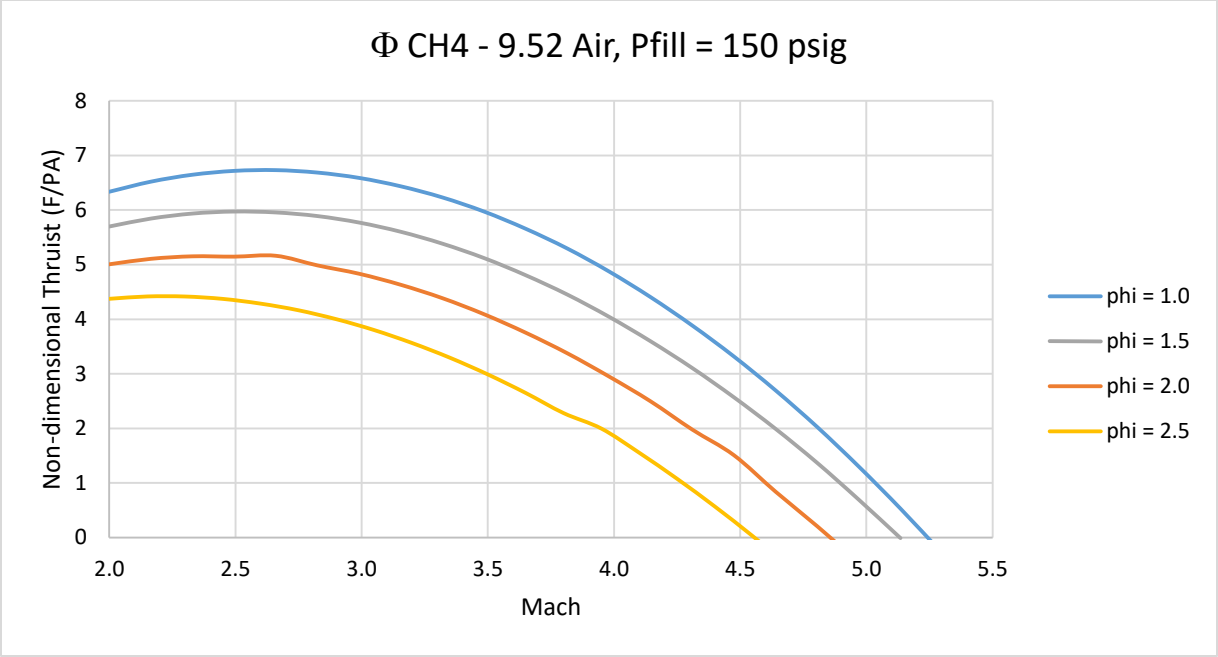

Figure 4. 14: TCRA theoretical thrust/heat release-Mach curve (1.0 CH4 + 9.52 Air; P = 150psi/10atm)

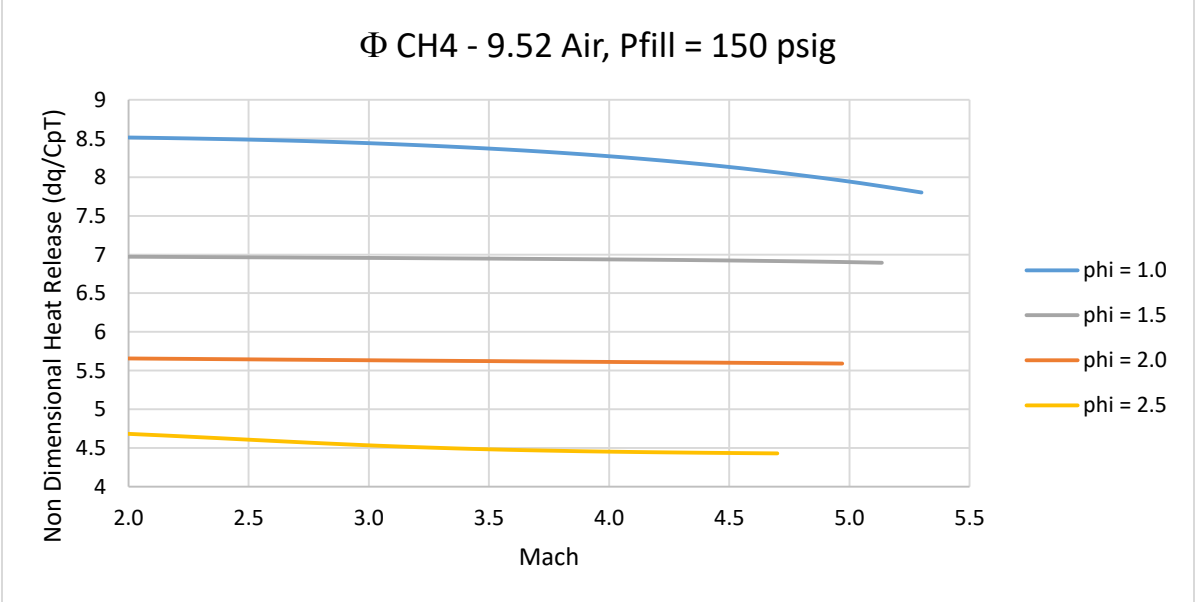

Figure 4. 15: Non-dimensional heat release of the RTRA propellants

CHAPTER 5: CONCLUSION

The prototype RTRA in UW was proven to be a valid system to obtain hypersonic launch velocity in the future. The initial operation envelop of the RTRA was explored and the result indicated that the RTRA was able to operate at a propellant mixture of 1.0 CH_4 + 9.52 Air. The projectile in the RTRA was able to gain additional velocity as the fill pressure was increased. The RTRA was also found to have a promising potential of low speed start operation in CH4/Air propellants. However, the current prototype railed-tube insert hardware was not able to withstand the high pressure generated by the wave unstart process in a mixture of 1.0 CH_4 + 9.52 Air at 225 psig (16 atm).

The initial experiments on the prototype RTRA were too limited in number to make any firm conclusions. The non-dimensional thrust of the current RTRA system measured in the experiments was only a fraction of theoretical non-dimensional thrust of the TCRA system. This indicated that the TCRA propulsive mode was not established in these experiments, possibly because the starting transient requires more than 2-m to enable a successful start. The prototype RTRA required a more energetic propellant to achieve combustion than used in the SBRA, although it is not yet clear whether this is due to too low of entrance velocity or the large flow area around the projectile throat.

Future Work

The initial experiment result on the prototype RTRA offers an insight of the potential of this system. There is plenty of study and research that can be conducted on the operational envelope and axis-symmetric projectile performance. Based on the experiences of this RTRA project, the following future work is recommended:

- Redesign railed-tube insert without the need of centering rings and ‘floating rails’ (current solution)
- Extend the length of the railed-tube insert such that the current adaptive collars are not required
- Explore methane/air propellant mixture with higher non-dimensional heat release, i.e., oxygen-rich air at 150 psi (10atm)
- Increase filled pressure beyond 225 psig (16 atm) on the current initial working propellant mixture to explore the relationship between projectile velocity gain and filled pressure
- Perform inert gas (nitrogen) RTRA shot to understand the baseline behavior of the system – drag profile of the current projectile in the RTRA
- Perform CFD analysis on the RTRA with inert gas model

BIBLIOGRAPHY

[1] Hertzberg, A., Bruckner, A.P., Bogdanoff, D.W., "Ram Accelerator: A New Chemical Method for Accelerating Projectiles to Ultrahigh Velocities," *AIAA Journal*, Vol. 26, No. 2, pp. 195-203, 1988.

[2] Hertzberg, A., Bruckner, A.P., Bogdanoff, D.W., Knowlen, C., "Operational Characteristics of the Thermally Choked Ram Accelerator," *Journal of Propulsion and Power*, Vol. 7, No. 5, pp. 828-836, 1991.

[3] Bruckner, A.P. and Knowlen, C., "The Ram Accelerator: Review of Experimental Research Activities in the U.S," *Experimental Methods of Shock Wave Research*, Vol. 9, Igra, O. and Seiler, F. (eds.), Springer-Verlag, Berlin, pp. 79–110, 2016.

[4] Bruckner, A.P., "The Ram Accelerator: A Technology Overview," AIAA 2002-1014, 40th Aerospace Sciences Meeting and Exhibit, Reno, NV, January 14-17, 2002

[5] Higgins, A.J., Knowlen, C. and Kiyanda, C.B., "Gasdynamic Operation of Baffled Tube Ram Accelerator in Highly Energetic Mixtures," 20th International Colloquium on the Dynamics of Explosions and Reactive Systems, Montreal, Canada, August 31 – Sept. 5, 2005.

[6] Higgins, A.J., "Ram Accelerators: Outstanding Issues and New Directions," *Journal of Propulsion and Power*, Vol. 22, No. 6, pp. 1170-1187, 2006.

[7] Knowlen, C., Glusman, J., Grist, R., Bruckner, A.P., and Higgins, A.J., "Experimental Investigation of a Baffled-Tube Ram Accelerator," AIAA 2016-4813, AIAA Propulsion and Energy Forum, Salt Lake City, UT, July 25-27, 2016

[8] Glusman, J., “Theoretical Performance Model and Initial Experimentation of a Baffled-Tube Ram Accelerator," MSAA thesis, University of Washington, 2016.

[9] Byrd, T., “Experimentally-Driven Model for the Based-Tube Ram Accelerator," MSAA thesis, University of Washington, 2018.

[10] Knowlen, C., Byrd, T., Dumas, J., Daneshvaran, N., Glusman, J., Grist, R., Bruckner, A.P., and Higgins, A.J., “Baffled-Tube Ram Accelerator Operation with Inclined Baffles,” AIAA 2017-4959, AIAA Propulsion and Energy Forum, Atlanta GA, July 10-12, 2017.

[11] Knowlen, C. and Bruckner, A.P., “Direct Space Launch Using Ram Accelerator Technology,” *Space Technology and Applications Forum–2001*, El-Genk, M.S., ed., pp. 583-588, American Institute of Physics, Albuquerque, NM, February 11-14, 2001.

[12] Knowlen, C., Joseph, B., and Bruckner, A.P., “Ram Accelerator as an Impulsive Space Launcher: Assessment of Technical Risks,” International Space Development Conference (invited), Dallas, TX, May 25-28, 2007.

[13] Seiler, F., Patz, G., Smeets, G., Srulijes, J., “Progress of ram acceleration with ISL’s RAMAC 30”, *Journal de Physique IV France*, 10:31-40, 2000.

[14] Private communication with Mark Russell, CEO of HyperSciences, LLC, 2013.

[15] Schultz, E., Knowlen, C., Bruckner, A., “Starting Envelope of the Subdetonative Ram Accelerator," *Journal of Propulsion and Power*, Vol. 14, No. 6, 2000, pp. 1040-1052.

[16] Knowlen, C., “Theoretical and Experimental Investigation of the Thermodynamics of the Thermally Choked Ram Accelerator," Ph.D. dissertation, University of Washington, 1991.

[17] Higgins, A. J., Knowlen, C., and Bruckner, A. P., “Ram Accelerator Operating Limits, Part 1: Identication of Limits," *Journal of Propulsion and Power*, Vol. 14, No. 6, 1998, pp. 951-958.

[18] Higgins, A. J., Knowlen, C., and Bruckner, A. P., “Ram Accelerator Operating Limits, Part 2: Nature of Observed Limits," *Journal of Propulsion and Power*, Vol. 14, No. 6, Nov. - Dec., 1998, pp. 959-966.